

---

# InfoBridge: Mutual Information estimation via Bridge Matching

---

**Sergei Kholkin**

Skoltech\*  
Moscow, Russia  
s.kholkin@skoltech.ru

**Ivan Butakov**

Skoltech\*, MIPT†  
Moscow, Russia  
butakov.id@phystech.edu

**Evgeny Burnaev**

Skoltech\*, AIRI‡  
Moscow, Russia  
e.burnaev@skoltech.ru

**Nikita Gushchin**

Skoltech\*, AIRI‡  
Moscow, Russia  
n.gushchin@skoltech.ru

**Alexander Korotin**

Skoltech\*, AIRI‡  
Moscow, Russia  
a.korotin@skoltech.ru

## Abstract

Diffusion bridge models have recently become a powerful tool in the field of generative modeling. In this work, we leverage their power to address another important problem in machine learning and information theory, the estimation of the mutual information (MI) between two random variables. We show that by using the theory of diffusion bridges, one can construct an unbiased estimator for data posing difficulties for conventional MI estimators. We showcase the performance of our estimator on two standard MI estimation benchmarks, i.e., low-dimensional and image-based, and on real-world data, i.e., protein language model embeddings.

## 1 Introduction

Information theory offers an extensive set of tools for quantifying probabilistic relations between random variables. It is widely used in machine learning for advanced statistical analysis [7, 68, 24, 10], assessment of deep neural networks’ performance and generalization capabilities [76, 86, 32, 73, 1, 14], self-supervised and semi-supervised learning [55, 6, 37, 75, 4, 83, 80, 78] and regularization or alignment in generative modeling [15, 5, 3, 84].

The majority of the aforementioned applications revolve around one of the central information-theoretic quantities – *mutual information* (MI). Due to several outstanding properties, MI is widely used as an invariant measure of non-linear dependence between random variables. Unfortunately, recent studies suggest that the curse of dimensionality is highly pronounced when estimating MI [29, 57]. Additionally, it is argued that long tails, high values of MI and some other particular features of complex probability distributions can make mutual information estimation even more challenging [18]. On the other hand, recent developments in neural estimation methods demonstrate that sophisticated parametric estimators can achieve notable practical success in situations where traditional mutual information estimation techniques struggle [5, 80, 71, 62, 2, 13]. Among neural estimators, generative approaches are of particular interest, as they have proven to be effective in handling complex data [23, 28, 13]. Since MI estimation is closely tied to approximation of a joint probability distribution, one can argue that leveraging state-of-the-art generative models, e.g., diffusion models, may result in additional performance gains.

---

\*Skolkovo Institute of Science and Technology

†Moscow Institute of Physics and Technology

‡Artificial Intelligence Research Institute

**Diffusion Bridge Matching.** Diffusion models are a powerful type of generative models that show an impressive quality of image generation [38, 63]. However, they have some disadvantages, such as the inability to perform data-to-data translation via diffusion. To tackle this problem, a novel promising approach based on Reciprocal Processes [54] and Schrödinger Bridges theory [67, 52] have emerged. This approach is called the *diffusion bridge matching* and is used for learning generative models as diffusion processes for data-to-data translation. This type of models has shown itself as a powerful approach for numerous applications in biology [77, 12], chemistry [70, 42], computer vision [56, 69, 88], speech processing [16] and unpaired learning [36, 34, 69].

**Contributions.** In this work, we employ the Diffusion Bridge Matching for the MI estimation.

1. **Theory.** We propose an unbiased mutual information estimator based on reciprocal processes, their diffusion representations and the Girsanov theorem (§4.1).
2. **Practice.** Building on the proposed theoretical framework and the powerful generative methodology of diffusion bridges, we develop a practical algorithm for MI estimation, named *InfoBridge* (§4.2). We demonstrate that our method achieves performance comparable to existing approaches on low-dimensional benchmarks and superior performance on image data benchmarks and protein embeddings data benchmark (§5).

**Notations.** We work in  $\mathbb{R}^D$ , which is the  $D$ -dimensional Euclidean space equipped with the Euclidean norm  $\|\cdot\|$ . We use  $\mathcal{P}(\mathbb{R}^D)$  to denote the absolutely continuous Borel probability distributions whose variance and differential entropy are finite. To denote the density of  $q \in \mathcal{P}(\mathbb{R}^D)$  at a point  $x \in \mathbb{R}^D$ , we use  $q(x)$ . We write  $\text{KL}(\cdot\|\cdot)$  to denote the Kullback-Leibler divergence between two distributions. We use  $\Omega$  to denote the space of trajectories, i.e., continuous  $\mathbb{R}^D$ -valued functions of  $t \in [0, 1]$ . We write  $\mathcal{P}(\Omega)$  to denote the probability distributions on the trajectories  $\Omega$  whose marginals at  $t = 0$  and  $t = 1$  belong to  $\mathcal{P}(\mathbb{R}^D)$ ; this is the set of stochastic processes. We use  $dW_t$  to denote the differential of the standard Wiener process  $W \in \mathcal{P}(\Omega)$ . We use  $Q_{|x_0}$  and  $Q_{|x_0, x_1}$  to denote the distribution of stochastic process  $Q$  conditioned on  $Q$ 's values  $x_0$  and  $x_0, x_1$  at times  $t = 0$  and  $t = 0, 1$ , respectively. For a process  $Q \in \mathcal{P}(\Omega)$ , we denote its marginal distribution at time  $t$  by  $q(x_t) \in \mathcal{P}(\mathbb{R}^D)$ , and if the process is conditioned on its value  $x_s$  at time  $s$ , we denote the marginal distribution of such a process at time  $t$  by  $q(x_t|x_s) \in \mathcal{P}(\mathbb{R}^D)$ .

## 2 Background

**Mutual information.** Information theory is a well-established framework for analyzing and quantifying interactions between random vectors. In this framework, mutual information (MI) serves as a fundamental and invariant measure of the non-linear dependence between two  $\mathbb{R}^D$ -valued random vectors  $X_0, X_1$ . It is defined as follows:

$$I(X_0; X_1) \stackrel{\text{def}}{=} \text{KL}(\Pi_{X_0, X_1} \|\Pi_{X_0} \otimes \Pi_{X_1}), \quad (1)$$

where  $\Pi_{X_0, X_1}$  and  $\Pi_{X_0}, \Pi_{X_1}$  are the joint and marginal distributions of a pair of random vectors  $(X_0, X_1)$ . If the corresponding PDF  $\pi(x_0, x_1)$  exists, the following also holds:

$$I(X_0; X_1) = \mathbb{E}_{\pi(x_0, x_1)} \log \frac{\pi(x_0, x_1)}{\pi(x_0)\pi(x_1)}. \quad (2)$$

Mutual information is symmetric, non-negative and equals zero if and only if  $X_0$  and  $X_1$  are independent. MI is also invariant to bijective mappings:  $I(X_0; X_1) = I(g(X_0); X_1)$  if  $g^{-1}$  exists and  $g, g^{-1}$  are measurable [17, 61].

**Brownian Bridge.** Let  $W^\epsilon$  be the Wiener process with a constant volatility  $\epsilon > 0$ , i.e., it is described by the SDE  $dW^\epsilon = \sqrt{\epsilon}dW_t$ , where  $W_t$  is the standard Wiener process. Let  $W_{|x_0, x_1}^\epsilon$  denote the process  $W^\epsilon$  conditioned its on values  $x_0, x_1$  at times  $t = 0, 1$ , respectively. This process  $W_{|x_0, x_1}^\epsilon$  is called the Brownian Bridge [41, Chapter 9].

**Reciprocal processes.** Reciprocal processes are a class of stochastic processes that have recently gained attention of research community in the contexts of stochastic optimal control [54], Schrödinger

Bridges [67, 52] and diffusion generative modeling [56, 34]. In our paper, we consider a *particular case* of reciprocal processes which are induced by the Brownian Bridge  $W_{|x_0, x_1}^\epsilon$ .

Consider a joint distribution  $\pi(x_0, x_1) \in \mathcal{P}(\mathbb{R}^{D \times 2})$  and define the process  $Q_\pi \in \mathcal{P}(\Omega)$  as a mixture of Brownian bridges  $W_{|x_0, x_1}^\epsilon$  with weights  $\pi(x_0, x_1)$ :

$$Q_\pi \stackrel{\text{def}}{=} \int W_{|x_0, x_1}^\epsilon d\pi(x_0, x_1).$$

This implies that to get trajectories of  $Q_\pi$  one has to first sample the start and end points,  $x_0$  and  $x_1$ , at times  $t = 0$  and  $t = 1$  from  $\pi(x_0, x_1)$  and then simulate the Brownian Bridge  $W_{|x_0, x_1}^\epsilon$ . Due to the non-causal nature of trajectory formation, such a process is, in general, non markovian. The set of all mixtures of Brownian Bridges can be described as:

$$\{Q \in \mathcal{P}(\Omega) \text{ s.t. } \exists \pi \in \mathcal{P}(\mathbb{R}^{D \times 2}) : Q = Q_\pi\}$$

and is called the set of *reciprocal processes* (for  $W^\epsilon$ ).

**Reciprocal processes conditioned on the point.** Consider a reciprocal process  $Q_\pi$  conditioned on some start point  $x_0$ . Let the resulting process be denoted as  $Q_{\pi|x_0}$ , which remains reciprocal. Then, if some regularity assumptions are met [69, Appx C.1] process  $Q_{\pi|x_0}$  is known as the Schrödinger Föllmer process [40, 81]. While  $Q_\pi$  itself is, in general, not markovian,  $Q_{\pi|x_0}$  **is markovian**. Furthermore, it is a diffusion process governed by the following SDE:

$$\begin{aligned} Q_{\pi|x_0} : dx_t &= v_{x_0}(x_t, t)dt + \sqrt{\epsilon}dW_t, x_0 \sim \delta(x_0), \\ v_{x_0}(x_t, t) &= \mathbb{E}_{q_\pi(x_1|x_t, x_0)} \left[ \frac{x_1 - x_t}{1 - t} \right]. \end{aligned} \quad (3)$$

**Representations of reciprocal processes.** The process  $Q_\pi$  can be naturally represented as a mixture of processes  $Q_{\pi|x_0}$  conditioned on their starting points  $x_0$ :

$$Q_\pi = \int Q_{\pi|x_0} d\pi(x_0).$$

Therefore, one may also express  $Q_\pi$  via an SDE but with non-markovian drift (conditioned on  $x_0$ ):

$$\begin{aligned} Q_\pi : dx_t &= v(x_t, t, x_0)dt + \sqrt{\epsilon}dW_t, x_0 \sim \pi(x_0), \\ v(x_t, t, x_0) &= v_{x_0}(x_t, t) = \mathbb{E}_{q_\pi(x_1|x_t, x_0)} \left[ \frac{x_1 - x_t}{1 - t} \right]. \end{aligned} \quad (4)$$

**Conditional Bridge Matching.** Although the drift  $v_{x_0}(x_t, t)$  of  $Q_{\pi|x_0}$  in (3) admits a closed form, it usually cannot be computed or estimated directly due to the unavailability of a way to easily sample from  $\pi(x_1|x_t, x_0)$ . However, it can be recovered by solving the following regression problem [88]:

$$v_{x_0} = \arg \min_u \mathbb{E}_{q_\pi(x_1, x_t|x_0)} \left\| \frac{x_1 - x_t}{1 - t} - u(x_t, t) \right\|^2, \quad (5)$$

which optimizes over drifts  $u : \mathbb{R}^D \times [0, 1] \rightarrow \mathbb{R}^D$ . The same holds for the  $Q_\pi$  and its drift  $v(x_t, t, x_0)$  through the addition of expectation w.r.t.  $\pi(x_0)$ :

$$v = \arg \min_u \mathbb{E}_{q_\pi(x_1, x_t|x_0)\pi(x_0)} \left\| \frac{x_1 - x_t}{1 - t} - u(x_t, t, x_0) \right\|^2 = \arg \min_u \mathbb{E}_{q_\pi(x_1, x_t, x_0)} \left\| \frac{x_1 - x_t}{1 - t} - u(x_t, t, x_0) \right\|^2,$$

where  $u : \mathbb{R}^D \times [0, 1] \times \mathbb{R}^D \rightarrow \mathbb{R}^D$ . Problem (2) is usually solved with standard deep learning techniques. Namely, one parametrizes  $u$  with a neural network  $v_\theta$ , and minimizes (2) using stochastic gradient descent and samples drawn from  $q_\pi(x_0, x_t, x_1)$ . The latter sampling is easy if one can sample from  $\pi(x_0, x_1)$ . Indeed,  $q_\pi(x_0, x_t, x_1) = q_\pi(x_t|x_0, x_1)\pi(x_0, x_1)$ , and one can sample first from  $\pi(x_0, x_1)$  and then from  $q_\pi(x_t|x_0, x_1)$ , which is just the Brownian Bridge [48, Eq 14].

Such a procedure of learning drift  $v$  with a neural network is popular in generative modeling to solve a problem of sampling from conditional distribution  $\pi(x_1|x_0)$  and is frequently applied in the image-to-image transfer [56]. The procedure of learning drift  $v(x_t, t, x_0)$  (2) is usually called the *conditional* (or augmented) *bridge matching* [21, 88]. In addition, such procedure can also be derived through the well-celebrated Doob  $h$ -transform [21, 88, 59] or reversing a diffusion [88].

**KL divergence between diffusion processes.** Consider two diffusion processes with the same volatility coefficient  $\sqrt{\epsilon}$  that start at the same distribution  $\pi_0$ :

$$\begin{aligned} Q^A : dx_t &= f^A(x_t, t)dt + \sqrt{\epsilon}dW_t, x_0 \sim \pi_0(x_0) \\ Q^B : dx_t &= f^B(x_t, t)dt + \sqrt{\epsilon}dW_t, x_0 \sim \pi_0(x_0) \end{aligned}$$

By the application of the disintegration theorem [53, §1] and the Girsanov theorem [58, §8.6] one can derive the KL divergence between these diffusions:

$$\text{KL}(Q^A \| Q^B) = \frac{1}{2\epsilon} \int_0^1 \mathbb{E}_{q^A(x_t)} [\|f^A(x_t, t) - f^B(x_t, t)\|^2] dt, \quad (6)$$

where  $q^A(x_t)$  is the marginal distribution of  $Q^A$  at time  $t$ .

This allows one to estimate the KL divergence between two diffusions with the same volatility coefficient and the same initial distributions, knowing only their *drifts* and marginal samples  $x_t \sim q^A(x_t)$ . This fact is widely used in Bridge Matching [69, 60], Diffusion [28] and Schrödinger Bridge Models [82, 35].

### 3 Related Work

**Mutual information estimators.** Mutual information estimators fall into two main categories: *non-parametric* and *parametric*. Parametric estimators are also subdivided into *discriminative* and *generative* [71, 27]. In addition to this natural classification, we distinguish *diffusion-based* approaches to better contextualize our method in relation to the previous works.

**Non-parametric estimators.** Classical approaches to the mutual information estimation rely on non-parametric density estimators, such as kernel density estimator [85, 32] and  $k$ -nearest neighbors estimator [49, 50, 8]. The resulting density estimate is plugged into (2) to acquire the MI estimate through MC-integration, leave-one-out method or other techniques. The simplicity of such methods make them appealing for low-dimensional cases, but extensive high-dimensional evaluation suggests that these approaches are inapplicable to complex data (32, § 5.3; 18, § 6.2; 13, Table 1).

**Non-diffusion-based generative estimators.** More advanced techniques involve parametric density models, such as normalizing flows and variational autoencoders, to measure MI through density estimation. This naïve generative approach was described by [71, 57] and further investigated in the works of [2, 23]. However, despite better modeling capabilities, the results in [71, Figures 1,2] indicate that direct PDF estimation can introduce a substantial bias to the MI estimate. Therefore, it was proposed to avoid PDF estimation altogether and focus on measuring the density ratio in (2). This is done in the works of [23, 13, 20] by leveraging the invariance property of mutual information. Such methods show better performance on synthetic benchmarks, but may introduce an inductive bias due to the simplified closed-form expression being used to estimate the density ratio in question.

**Discriminative estimators.** Finally, another approach to MI estimation involves training a classifier to discriminate between the samples from  $\pi(x_0, x_1)$  and  $\pi(x_0)\pi(x_1)$ : MINE [5], InfoNCE [80] and similar methods [71]. This technique leverages variational bounds on the Kullback-Leibler divergence and provides a relatively cheap and reliable parametric estimator for a wide range of cases, including high-dimensional and complex data. However, such estimators have severe demerits from a theoretical perspective, such as high variance in MINE and large batch size requirements in InfoNCE [71]. Additionally, recent benchmarking results suggest that discriminative approaches can underperform compared to the generative methods when MI is high and the probability distribution is complex [28, 13].

**Neural Diffusion Estimator for MI (MINDE).** One of the most recent generative methods for MI Estimation is diffusion-based [72] MINDE [28]. To estimate  $\text{KL}(\pi^A \| \pi^B)$  the authors learn two standard backward diffusion models to generate data from distributions  $\pi^A$  and  $\pi^B$ , e.g., for  $\pi^A$ :

$$Q^A : dx_t = \underbrace{[-f(x_t, t) + g(t)^2 s^A(x_t, t)]dt + g(t)d\hat{W}_t}_{\text{backward diffusion}}, \quad x_T \sim q_T^A(x_T), \quad (7)$$

where  $f$  and  $g$  are the drift and volatility coefficients, respectively, of the forward diffusion [72],  $d\hat{W}_t$  is the Wiener process when time flows backwards, and  $q_t^A$  is the distribution of the noised data at

time  $t$  [28, §2, 3]. The similar expressions hold for  $\pi^B$  and  $Q^B$ . Then, the authors formulate a KL divergence estimator through the difference of diffusion *score functions*:

$$\text{KL}(\pi^A \parallel \pi^B) = \text{KL}(Q^A \parallel Q^B) = \int_0^T \mathbb{E}_{q_t^A(x_t)} \left[ \frac{g(t)^2}{2} \|s^A(x_t, t) - s^B(x_t, t)\|^2 \right] dt + \text{KL}(q_T^A \parallel q_T^B). \quad (8)$$

Here,  $\text{KL}(q_T^A \parallel q_T^B)$  is the **bias** term, which vanishes only when diffusion has infinitely many steps, i.e.,  $T \rightarrow \infty$ . When the diffusion score functions  $s^A$  and  $s^B$  (7) are properly learned, one can draw samples from the forward diffusion  $q_t^A(x_t) = q_t^A(x_t|x_0)q(x_0)$  and compute the estimate of KL divergence (8). In this way, the authors transform the problem of training the KL divergence estimator into the problem of learning the backward diffusions (7) that generate *data from noise*.

To estimate **mutual information**, the authors propose a total of four equivalent methods, all based on the estimation of up to three KL divergences (8) or their expectations.

## 4 InfoBridge Mutual Information estimator

In §4.1, we propose our novel MI estimator which is based on difference of diffusion drifts of conditional reciprocal processes. We explain the practical learning procedure in §4.2 and suggest some straightforward generalizations of our method in §4.3.

### 4.1 Computing MI through Reciprocal Processes

Consider the problem of MI estimation for random variables  $X_0$  and  $X_1$  with joint distribution  $\pi(x_0, x_1)$ . To tackle this problem, we employ reciprocal processes:

$$Q_\pi \stackrel{\text{def}}{=} \int W_{|x_0, x_1}^\epsilon d\pi(x_0, x_1), Q_\pi^{\text{ind}} \stackrel{\text{def}}{=} \int W_{|x_0, x_1}^\epsilon d\pi(x_0) d\pi(x_1). \quad (9)$$

We show that the KL between the distributions  $\pi(x_0, x_1)$  and  $\pi(x_0)\pi(x_1)$  (1) is equal to the KL between the reciprocal processes  $Q_\pi$  and  $Q_\pi^{\text{ind}}$ , and decompose the latter into the difference of drifts.

**Theorem 4.1** (Mutual Information decomposition). *Consider random variables  $X_0, X_1$ , that satisfy some regularity assumptions, [69, Appendix C], with joint distribution  $\pi(x_0, x_1)$ . Consider reciprocal processes  $Q_\pi, Q_\pi^{\text{ind}}$  induced by distributions  $\pi(x_0, x_1)$  and  $\pi(x_0)\pi(x_1)$ , respectively, as in (9). Then the mutual information between the random variables  $X_0$  and  $X_1$  can be expressed as:*

$$I(X_0; X_1) = \frac{1}{2\epsilon} \int_0^1 \mathbb{E}_{q_\pi(x_t, x_0)} \|v_{\text{joint}}(x_t, t, x_0) - v_{\text{ind}}(x_t, t, x_0)\|^2 dt, \quad (10)$$

where

$$v_{\text{joint}}(x_t, t, x_0) = \mathbb{E}_{q_\pi(x_1|x_t, x_0)} \left[ \frac{x_1 - x_t}{1 - t} \right], \quad (11)$$

$$v_{\text{ind}}(x_t, t, x_0) = \mathbb{E}_{q_\pi^{\text{ind}}(x_1|x_t, x_0)} \left[ \frac{x_1 - x_t}{1 - t} \right]. \quad (12)$$

$v_{\text{joint}}$  and  $v_{\text{ind}}$  are the drifts of the SDE representations (4) of the reciprocal processes  $Q_\pi$  and  $Q_\pi^{\text{ind}}$ .

*Proof.* Using the disintegration theorem [53, §1] at time  $t = 0$ , we get:

$$\text{KL}(Q_\pi \parallel Q_\pi^{\text{ind}}) = \text{KL}(\pi(x_0) \parallel \pi(x_0)) + \mathbb{E}_{\pi(x_0)} [\text{KL}(Q_{\pi|x_0} \parallel Q_{\pi|x_0}^{\text{ind}})].$$

Note that since  $Q_\pi, Q_\pi^{\text{ind}}$  share the same marginals at time  $t = 0$ , first KL term vanishes. Similarly, by using the disintegration theorem again for both times  $t = 0, 1$ , we get:

$$\text{KL}(Q_\pi \parallel Q_\pi^{\text{ind}}) = \text{KL}(\pi(x_0, x_1) \parallel \pi(x_0)\pi(x_1)) + \mathbb{E}_{\pi(x_0, x_1)} [\text{KL}(Q_{\pi|x_0, x_1} \parallel Q_{\pi|x_0, x_1}^{\text{ind}})].$$

Recap that  $Q_\pi$  and  $Q_\pi^{\text{ind}}$  are both mixtures of Brownian Bridges. Therefore,  $Q_{\pi|x_0, x_1} = Q_{\pi|x_0, x_1}^{\text{ind}} = W_{|x_0, x_1}^\epsilon$  and  $\text{KL}(Q_{\pi|x_0, x_1} \parallel Q_{\pi|x_0, x_1}^{\text{ind}}) = 0$ . Then the following holds:

$$\text{KL}(Q_\pi \parallel Q_\pi^{\text{ind}}) = \text{KL}(\pi(x_0, x_1) \parallel \pi(x_0)\pi(x_1)) = \mathbb{E}_{\pi(x_0)} [\text{KL}(Q_{\pi|x_0} \parallel Q_{\pi|x_0}^{\text{ind}})].$$

Moreover, processes  $Q_{\pi|x_0}$  and  $Q_{\pi|x_0}^{\text{ind}}$  are diffusion processes (§2). Then, by recalling (6), we get:

$$\text{KL}(\pi(x_0, x_1) \parallel \pi(x_0)\pi(x_1)) = \mathbb{E}_{\pi(x_0)} [\text{KL}(Q_{\pi|x_0} \parallel Q_{\pi|x_0}^{\text{ind}})] = \quad (13)$$

$$\frac{1}{2\epsilon} \int_0^1 \mathbb{E}_{q_\pi(x_t, x_0)} [\|v_{\text{joint}}(x_t, t, x_0) - v_{\text{ind}}(x_t, t, x_0)\|^2] dt,$$

where drifts  $v_{\text{joint}}$  and  $v_{\text{ind}}$  are defined as in (11) and (12) respectively.  $\square$

---

**Algorithm 1:** *InfoBridge*. Training the model.

---

**Input** : Distribution  $\pi(x_0, x_1)$  accessible by samples, initial neural network parametrization  $v_\theta$  of drift functions

**Output** : Learned neural network  $v_\theta$  approximating drifts  $v_{\text{joint}}$  and  $v_{\text{ind}}$

**repeat**

Sample batch of pairs  $\{x_0^n, x_1^n\}_{n=0}^N \sim \pi(x_0, x_1)$ ;  
 Sample random permutation  $\{\hat{x}_1^n\}_{n=0}^N = \text{Permute}(\{x_1^n\}_{n=0}^N)$ ;  
 Sample batch  $\{t^n\}_{n=1}^N \sim U[0, 1]$ ;  
 Sample batch  $\{x_t^n\}_{n=1}^N \sim W_{|x_0, x_1}^\epsilon$ ;  
 Sample batch  $\{\hat{x}_t^n\}_{n=1}^N \sim W_{|x_0, \hat{x}_1}^\epsilon$ ;  
 $\mathcal{L}_\theta^1 = \frac{1}{N} \sum_{n=1}^N \|v_\theta(x_t^n, t^n, x_0^n, 1) - \frac{x_1^n - x_t^n}{1 - t^n}\|^2$ ;  
 $\mathcal{L}_\theta^2 = \frac{1}{N} \sum_{n=1}^N \|v_\theta(\hat{x}_t^n, t^n, x_0^n, 0) - \frac{\hat{x}_1^n - \hat{x}_t^n}{1 - t^n}\|^2$ ;  
 Update  $\theta$  using  $\frac{\partial \mathcal{L}_\theta^1}{\partial \theta} + \frac{\partial \mathcal{L}_\theta^2}{\partial \theta}$ ;

**until** converged;

---



---

**Algorithm 2:** *InfoBridge*. MI estimator.

---

**Input** : Distribution  $\pi(x_0, x_1)$  accessible by samples, neural network parametrization  $v_\theta$  of drift functions approximating optimal drifts  $v_{\text{joint}}$  and  $v_{\text{ind}}$ , number of samples  $N$

**Output** : Mutual information estimation  $\widehat{\text{MI}}$

Sample batch of pairs  $\{x_0^n, x_1^n\}_{n=1}^N \sim \pi(x_0, x_1)$ ;  
 Sample batch  $\{t^n\}_{n=1}^N \sim U[0, 1]$ ;  
 Sample batch  $\{x_t^n\}_{n=1}^N \sim W_{|x_0, x_1}^\epsilon$ ;  
 $\widehat{\text{MI}} \leftarrow \frac{1}{2\epsilon N} \sum_{n=0}^N \|v_\theta(x_t^n, t^n, x_0^n, 1) - v_\theta(x_t^n, t^n, x_0^n, 0)\|^2$

---

Once the drifts  $v_{\text{joint}}$  and  $v_{\text{ind}}$  are known, our Theorem 4.1 provides a straightforward way to estimate the mutual information between the random variables  $X_0$  and  $X_1$  by evaluating the difference between the drifts  $v_{\text{joint}}(x_t, t, x_0)$  (11) and  $v_{\text{ind}}(x_t, t, x_0)$  (12) at points  $x_0, x_t$  sampled from the distribution of the reciprocal process  $Q_\pi$  at times 0,  $t$ . Regularity assumptions [69, Appendix C] are relatively mild and common for diffusion bridges generative modeling, i.e., they include restrictions such as finite first moment.

#### 4.2 *InfoBridge*. Practical optimization procedure

The drifts  $v_{\text{joint}}$  and  $v_{\text{ind}}$  of reciprocal processes  $Q_\pi$  and  $Q_\pi^{\text{ind}}$  can be recovered by the conditional Bridge Matching procedure, see §2. We have to solve optimization problem (2) by parametrizing  $v_{\text{joint}}$  and  $v_{\text{ind}}$  with neural networks  $v_{\text{joint}, \phi}$  and  $v_{\text{ind}, \psi}$ , respectively, and applying Stochastic Gradient Descent on Monte Carlo approximation of (2). The sampling from the distribution  $q_\pi(x_t, x_0)$  of reciprocal process  $Q_\pi$  at times 0,  $t$  is easy because:

$$q_\pi(x_t, x_0) = \mathbb{E}_{q_\pi(x_1)}[q_\pi(x_t, x_0|x_1)] = \mathbb{E}_{q_\pi(x_1)}[q_\pi(x_t|x_1, x_0)\pi(x_0|x_1)].$$

Therefore, to sample from  $q_\pi(x_t, x_0)$  it suffices to sample  $x_0, x_1 \sim \pi(x_0, x_1)$  and sample from  $q_\pi(x_t|x_1, x_0)$  which is again just a Brownian Bridge.

**Vector field parametrization.** In practice, we replace two separate neural networks that approximate the drifts  $v_{\text{joint}}(x_t, t, x_0)$  and  $v_{\text{ind}}(x_t, t, x_0)$  with a single neural network that incorporates an additional binary input. Specifically, we introduce a binary input  $s \in \{0, 1\}$  to unify the drift approximations in the following way:  $v_\theta(\cdot, 1) \approx v_{\text{joint}}(\cdot)$  and  $v_\theta(\cdot, 0) \approx v_{\text{ind}}(\cdot)$ . The introduction of an additional input is widely used for the conditioning of diffusion [39] and bridge matching [9] models. We have empirically found that it provides a much more accurate estimation of mutual information. We attribute its performance to the fact that for MI estimation we need to compute the difference between diffusion drifts (10). Neural networks do usually have some approximation error, then the difference between two almost identical neural networks with similar approximation errors is more accurate than the difference between two neural networks with distinct approximation errors.

We call our practical MI estimation algorithm ***InfoBridge***. The drifts  $v_\theta$  training procedure is described in Algorithm 1 and the MI estimation procedure is described in Algorithm 2.

Table 1: Mean MI estimates over 10 seeds using 10k test samples against ground truth (GT), adopted from [28]. Color indicates relative negative (red) and positive bias (blue). Size of train dataset for every neural method is 100k. All the methods for comparison, except for the NVF and JVF [20], were taken from [18, 28]. List of abbreviations (*Mn*: Multinormal, *St*: Student-t, *Nm*: Normal, *Hc*: Half-cube, *Sp*: Spiral). Methods explosion is abbreviated by  $\infty$ .

GT	Method Type	0.2	0.4	0.3	0.4	0.4	0.4	0.4	1.0	1.0	1.0	1.0	0.3	1.0	1.3	1.0	0.4	1.0	0.6	1.6	0.4	1.0	1.0	1.0	1.0	1.0	1.0	1.0	0.2	0.4	0.2	0.3	0.2	0.4	0.3	0.4	1.7	0.3	0.4			
<i>InfoBridge(ours)</i>	Bridge Matching	0.3	0.5	0.3	0.4	0.4	0.4	0.4	0.9	1.0	1.0	1.0	0.3	1.0	1.3	1.0	0.4	1.0	0.6	1.7	0.4	1.0	1.0	1.0	1.0	0.9	0.9	1.0	1.0	0.0	0.0	0.2	0.3	0.2	0.5	0.3	0.5	1.3	0.4	0.4		
NVF	Flow	0.2	0.4	0.3	0.6	0.4	0.4	0.4	1.0	1.0	1.0	1.0	0.3	1.0	1.3	1.0	0.4	1.0	0.6	1.5	0.4	1.0	1.0	1.0	0.8	0.5	0.6	0.9	1.0	1.0	∞	∞	0.0	0.5	0.2	-0.4	0.4	0.2	1.5	0.2	0.4	
JVF		0.0	0.0	0.0	0.0	0.4	0.4	0.4	1.0	1.0	1.0	1.0	0.3	1.0	1.3	1.0	0.4	1.0	0.6	1.6	0.4	1.0	1.0	1.0	0.8	0.3	0.4	1.0	0.9	0.9	1.8	2.7	0.0	0.1	0.0	0.0	1.6	0.2	0.4			
MINDE-J ( $\sigma = 1$ )	Diffusion	0.2	0.4	0.3	0.4	0.4	0.4	0.4	1.1	1.0	1.0	1.0	0.3	0.9	1.2	1.0	0.4	1.0	0.6	1.7	0.4	1.0	1.0	1.0	0.9	0.9	0.9	1.0	0.9	1.0	0.2	0.4	0.2	0.3	0.2	0.5	0.3	0.5	1.6	0.3	0.4	
MINDE-J		0.2	0.4	0.3	0.4	0.4	0.4	0.4	1.2	1.0	1.0	1.0	0.3	1.0	1.3	1.0	0.4	1.0	0.6	1.7	0.4	1.1	1.0	1.0	1.0	0.9	0.9	1.1	1.0	1.0	0.1	0.2	0.2	0.3	0.2	0.5	0.3	0.4	1.7	0.3	0.4	
MINDE-c ( $\sigma = 1$ )		0.2	0.4	0.3	0.4	0.4	0.4	0.4	1.0	1.0	1.0	1.0	0.3	1.0	1.3	1.0	0.4	1.0	0.6	1.6	0.4	0.9	1.0	1.0	1.0	0.9	0.9	0.9	1.0	0.9	0.1	0.3	0.2	0.3	0.2	0.4	0.3	0.3	1.7	0.3	0.4	
MINDE-c		0.2	0.4	0.3	0.4	0.4	0.4	0.4	1.0	1.0	1.0	1.0	0.3	1.0	1.3	1.0	0.4	1.0	0.6	1.6	0.4	1.0	1.0	1.0	1.0	0.9	0.9	0.9	1.0	1.0	1.0	0.1	0.3	0.2	0.3	0.2	0.4	0.3	0.4	1.7	0.3	0.4
MINE	Classical	0.2	0.4	0.2	0.4	0.4	0.4	0.4	1.0	1.0	1.0	1.0	0.3	1.0	1.3	1.0	0.4	1.0	0.6	1.6	0.4	0.9	0.9	0.9	0.8	0.7	0.6	0.9	0.9	0.9	0.0	0.0	0.1	0.1	0.1	0.2	0.2	0.4	1.7	0.3	0.4	
InfoNCE		0.2	0.4	0.3	0.4	0.4	0.4	0.4	1.0	1.0	1.0	1.0	0.3	1.0	1.3	1.0	0.4	1.0	0.6	1.6	0.4	0.9	1.0	1.0	0.8	0.8	0.8	0.9	1.0	1.0	0.2	0.3	0.2	0.3	0.2	0.4	0.3	0.4	1.7	0.3	0.4	
D-V		0.2	0.4	0.3	0.4	0.4	0.4	0.4	1.0	1.0	1.0	1.0	0.3	1.0	1.3	1.0	0.4	1.0	0.6	1.6	0.4	0.9	1.0	1.0	0.8	0.8	0.8	0.9	1.0	1.0	0.0	0.0	0.1	0.1	0.2	0.2	0.4	1.7	0.3	0.4		
NWJ		0.2	0.4	0.3	0.4	0.4	0.4	0.4	1.0	1.0	1.0	1.0	0.3	1.0	1.3	1.0	0.4	1.0	0.6	1.6	0.4	0.9	1.0	1.0	0.8	0.8	0.8	0.9	1.0	1.0	0.0	0.0	0.0	-0.6	0.1	0.1	0.2	0.2	0.4	1.7	0.3	0.4
DoE (Gaussian)		0.2	0.5	0.3	0.6	0.4	0.4	0.4	0.7	1.0	1.0	1.0	0.4	0.7	1.3	1.0	0.6	0.9	1.3	0.4	0.7	1.0	1.0	1.0	0.5	0.6	0.6	0.7	0.8	6.7	7.9	1.8	2.5	0.6	4.2	1.2	1.6	0.1	0.4			
DoE (Logistic)		0.1	0.4	0.2	0.4	0.4	0.4	0.4	0.6	0.9	0.9	1.0	0.3	0.7	1.1	1.0	0.6	0.9	1.3	0.4	0.7	1.0	1.0	1.0	0.5	0.6	0.6	0.7	0.8	0.8	0.5	0.8	0.3	1.5	0.6	1.6	0.1	0.4				
DoE (Logistic)		0.2	0.4	0.2	0.2	0.4	0.4	0.4	0.2	0.9	0.7	1.0	0.3	0.2	1.1	1.0	0.4	0.7	1.3	0.4	0.7	1.0	1.0	1.0	0.5	0.6	0.6	0.7	0.8	0.8	0.5	0.8	0.3	1.5	0.6	1.6	0.1	0.4				
KSG		0.2	0.4	0.2	0.2	0.4	0.4	0.4	0.2	0.9	0.7	1.0	0.3	0.2	1.1	1.0	0.4	0.7	1.3	0.4	0.7	1.0	1.0	1.0	0.5	0.6	0.6	0.7	0.8	0.8	0.5	0.8	0.3	1.5	0.6	1.6	0.1	0.4				

### 4.3 Generalizations and implications

**Generalizations.** Our method admits several straightforward extensions. For completeness, we present a method for the unbiased estimation of the general KL divergence in Appendix B.1. According to the Theorem B.1 the KL divergence between any two distributions can be decomposed into the difference of diffusion drifts in similar way to (10). This results allows to estimate the differential entropy of a probability distribution, see Appendix B.2. Corresponding illustrative experiments are presented in Appendix B.3.

In addition, our method can be extended to estimate mutual information involving more than two random variables, known as interaction information (Appendix B.4). Practical procedures for these generalizations can also be derived in a similar way to §4.2.

**Generative byproduct.** Note that the learned drifts  $v_\theta(\cdot, 1)$  and  $v_\theta(\cdot, 0)$  define the distributions  $\pi_{\theta, \text{joint}}(x_1|x_0) \approx \pi(x_1|x_0)$  and  $\pi_{\theta, \text{ind}}(x_1|x_0) \approx \pi(x_1)$  as solutions to the corresponding SDEs (4). One can sample from these distributions by solving the related SDE (4) numerically, e.g., using the Euler-Maryama solver [47]. Samples generated this way for the Image based benchmark can be seen at Figure 4. This is unnecessary for our MI estimation, but can be considered as an additional feature.

## 5 Experiments

We test our method on a diverse set of benchmarks with already known ground truth value of MI. To cover low-dimensional cases, long-tailed distributions and some basic cases of data lying on a manifold, we employ the tests by [18]. Benchmarks from [14, 13] are used to assess the method on manifolds represented as images. Finally, to evaluate our method on real-world data, we use protein language model embeddings and adopt the benchmark construction procedure proposed in [51].

### 5.1 Low-dimensional benchmark.

The tests from [18] focus on low-dimensional distributions with tractable mutual information. Various mappings are also applied to make the distributions light- or heavy-tailed, or to non-linearly embed the data into an ambient space of higher dimensionality.

*InfoBridge* is tested with  $\epsilon = 1$  and a multi-layer dense neural network is used to approximate the drifts. Our computational complexity is comparable to MINDE [28]. For more details, please, refer to Appendix C. In each test, we perform 10 independent runs with 100k train set samples and 10k test set samples. The mean MI estimation results are reported in the top row of Tables 1 and 9.

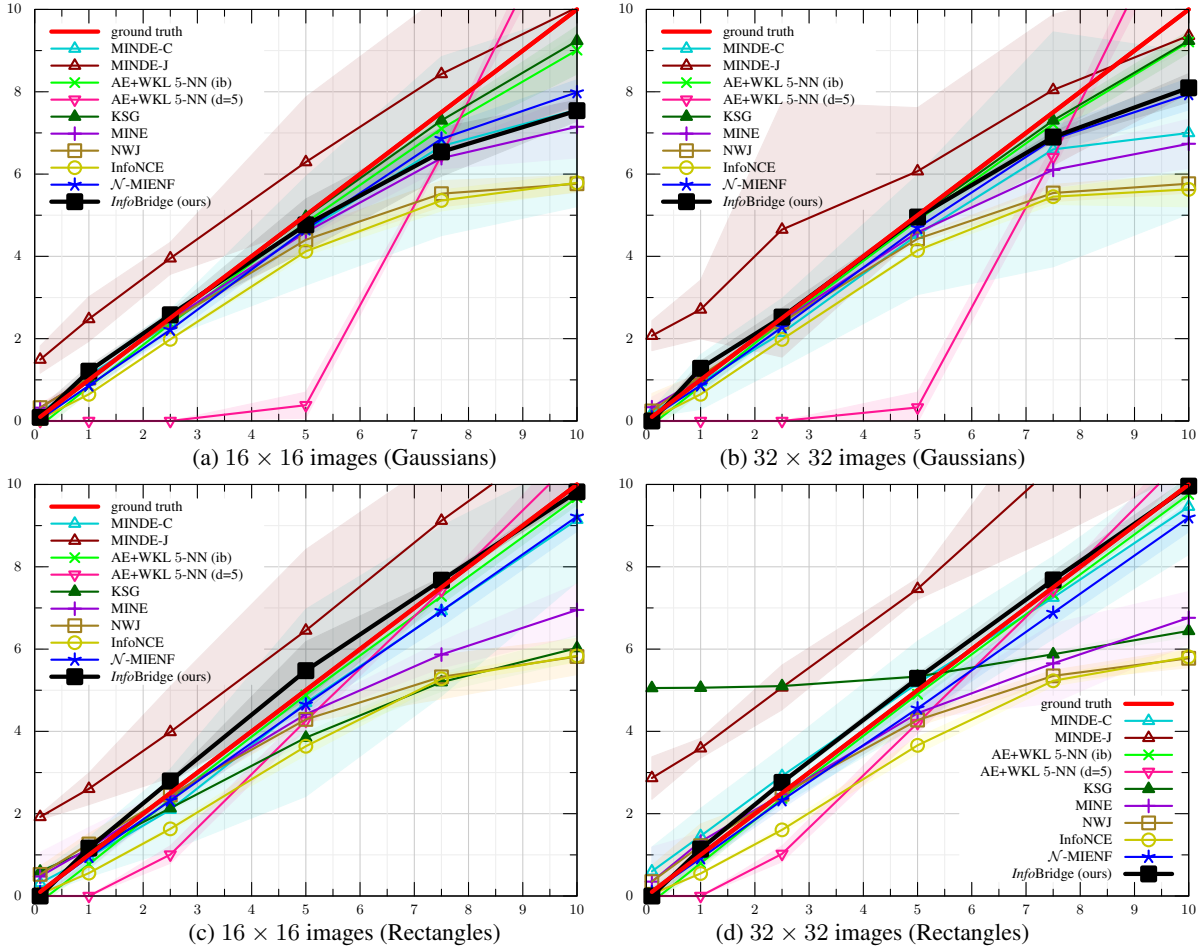


Figure 1: Comparison of the MI estimators. Along  $x$  axes is  $I(X_0; X_1)$ , along  $y$  axes is MI estimate  $\hat{I}(X_0; X_1)$ . We plot 99% confidence intervals acquired from different seed runs. Number of seeds for *InfoBridge*,  $\mathcal{N}$ -MIENF, MINDE is 3 and 5 for all the other methods. 100k samples were used for neural methods training and 10k for validation. MAE can be seen at Table 6. AE+WKL 5-NN (ib) and (d=5) stand for the versions with inductive bias and latent dimensionality of 5 respectively.

Overall, the performance of our estimator is similar to that of MINDE (§3) and superior to the classical and flow based, i.e., NVF and JFV [20], methods, with the Cauchy distribution (i.e., Student-t distribution with degrees of freedom equal to 1) being the only notable exception. Unfortunately, the Cauchy distribution lacks the first moment, which poses theoretical limitations for Bridge Matching [69, Appendix C]. More details about limitations are discussed in Appendix A. However, poor performance in Cauchy distribution case is the common MI estimators problem and by using the tail-shortening asinh transform allows our method to negate this issue and to estimate MI almost accurately, see first two Asinh columns in Tables 1 and 9.

## 5.2 Image data benchmark.

In [14], it was proposed to map low-dimensional distributions with tractable MI into manifolds admitting image-like structure, thus producing synthetic images (in particular, images of 2D Gaussians and Rectangles, see Figures 4a and 4b). By using smooth injective mappings, one ensures that MI is not alternated by the transform [13, Theorem 2.1]. In the original works, it is argued that such benchmarks are closer to real data, and therefore give more insights into the problems related to the MI estimation in realistic setups.

Each neural algorithm is trained with 100k train set samples and validated using 10k samples. *InfoBridge* is tested with  $\epsilon = 1$  and we use a neural network with U-net architecture [64] to approximate the drift. For averaging, we run algorithm with 3 different seeds. Other experimental details are reported in Appendix C.3 and the ablation study on neural network architecture and volatility coefficient  $\epsilon$  is presented in Appendix C.I.



We present our results for  $16 \times 16$  and  $32 \times 32$  resolution images with both Gaussian and rectangle structure in Figure 1 and MAE in Table 6, while the samples from the learned conditional bridge matching models can be viewed in Figures 4c to 4f. Our estimator looks very competitive, being consistently more precise and more stable than MINDE-C and MINDE-J and as good as or even better than two previous best-performing methods: MIENF [13] and 5-nearest neighbors weighted Kozachenko-Leonenko estimator [49, 8] fed with autoencoder-generated embeddings (AE+WKL 5-NN) [14]. We consider this to be a satisfactory outcome, since MIENF and AE+WKL utilize certain *prior information* about the test (specifically, the vector Gaussian copula structure in  $\mathcal{N}$ -MIENF [13, Section B, paragraph 1],<sup>4</sup> or the matching intrinsic dimensionality in AE+WKL<sup>5</sup>), while our estimator remains *free of any inductive bias*. Moreover, as a result of the tests conducted, we claim that our estimator is *the best among all inductive bias-free estimators* featured.

### 5.3 Protein embeddings data

We evaluate *InfoBridge* on real-world data, i.e., conduct experiments on protein language model embeddings. Following the benchmark construction method from [51], we generate paired datasets with known mutual information (MI) by ensuring that only class labels are shared between variables  $X$  and  $Y$ , making the MI analytically tractable [51, §4.5]. We use sequence embeddings from the ProtTrans5 model [25], based on proteins from *A. thaliana* and *H. sapiens*, to create datasets with varying ground truth MI. The final number of training pairs is 20641 and the dimensionality of embeddings is 1024. In addition, the ablation study on the volatility coefficient  $\epsilon$  is presented in Appendix C.1.

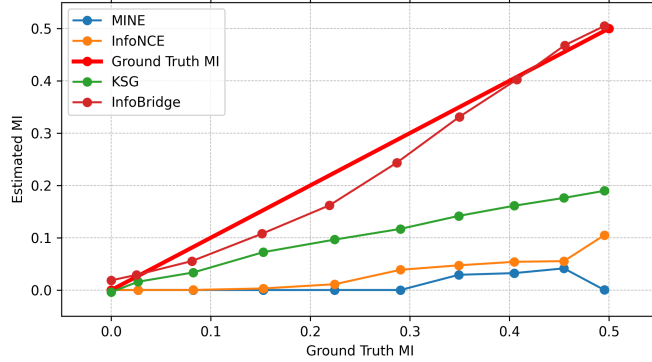


Figure 2: Comparison of the selected estimators on the ProtTrans5 data. Along  $x$  axes is ground truth  $I(X_0, X_1)$ , along  $y$  axes is MI estimate  $\hat{I}(X_0, X_1)$ . Results for *InfoBridge* averaged over last 5 MI estimations during training.

*InfoBridge* is trained for 100 epochs with similar to the low-dimensional benchmark (§5.1) hyperparameters. We compare against MINE, InfoNCE, KSG, and MINDE. All the [technical details](#) can be found in Appendix C.4. We present the results plot at Figure 2 and MAE at Table 8. One can see that *InfoBridge* is the only method to consistently estimate MI accurately; MINDE-C and MINDE-J are omitted as they drastically overestimate MI (e.g., MAE: MINDE-C 9.29 vs. *InfoBridge* 0.04).

## 6 Discussion

**Potential Impact.** Our contributions include the development of novel unbiased estimator for the MI grounded in diffusion bridge matching theory. The proposed algorithm, *InfoBridge*, demonstrates superior performance compared to commonly used MI estimators on both synthetic and real-world challenging high-dimensional benchmarks. Also, our approach can be used to estimate the KL divergence and differential entropy Appendices B.1 and B.2.

We believe that our work paves the way for new directions in the estimation of MI *in high dimensions*. This has potential real-world applications such as text-to-image alignment [84], self-supervised learning [4], deep neural network analysis [14], and other use cases in high-dimensional settings.

Moreover, our approach offers opportunities for extension by exploring alternative types of bridges within reciprocal processes, for instance, variance-preserving SDE bridges [88]. In addition, experimentation with advanced diffusion bridge techniques, such as time reweighting [44], could further

<sup>4</sup> $\mathcal{N}$ -MIENF requires  $\Pi_{X,Y}$  being gaussianizable via some Cartesian product mapping  $f_X \times f_Y$ ; the analysis provided in [19] suggests that this is a strong implication, which is extremely unlikely to be satisfied in non-synthetic cases.

<sup>5</sup>For the AE+WKL estimator, we use the experimental setup from [14], which skews the comparison against us since the autoencoder bottlenecks match the true intrinsic dimensionality of the data. Figure 1 and Table 6 shows the performance of the degraded performance of the method *without inductive bias*. Furthermore, we provide more information in Appendix C.5.

improve the methodology. Finally, for long-tailed data distributions, it may be possible to integrate long-tailed diffusion techniques [87], extending the applicability of our approach.

**Limitations.** We discuss limitations in Appendix A.

**Broader impact.** This paper presents work whose goal is to advance the field of Machine Learning. There are many potential societal consequences of our work, none of which we feel must be specifically highlighted here.

## References

- [1] Rana Ali Amjad, Kairen Liu, and Bernhard C. Geiger. Understanding neural networks and individual neuron importance via information-ordered cumulative ablation. *IEEE Transactions on Neural Networks and Learning Systems*, 33(12):7842–7852, 2022.
- [2] Ziqiao Ao and Jinglai Li. Entropy estimation via normalizing flow. *Proceedings of the AAAI Conference on Artificial Intelligence*, 36(9):9990–9998, Jun. 2022.
- [3] Lynton Ardizzone, Radek Mackowiak, Carsten Rother, and Ullrich Köthe. Training normalizing flows with the information bottleneck for competitive generative classification. In H. Larochelle, M. Ranzato, R. Hadsell, M.F. Balcan, and H. Lin, editors, *Advances in Neural Information Processing Systems*, volume 33, pages 7828–7840. Curran Associates, Inc., 2020.
- [4] Philip Bachman, R Devon Hjelm, and William Buchwalter. Learning representations by maximizing mutual information across views. In H. Wallach, H. Larochelle, A. Beygelzimer, F. d’Alché-Buc, E. Fox, and R. Garnett, editors, *Advances in Neural Information Processing Systems*, volume 32. Curran Associates, Inc., 2019.
- [5] Mohamed Ishmael Belghazi, Aristide Baratin, Sai Rajeshwar, Sherjil Ozair, Yoshua Bengio, Aaron Courville, and Devon Hjelm. Mutual information neural estimation. In Jennifer Dy and Andreas Krause, editors, *Proceedings of the 35th International Conference on Machine Learning*, volume 80 of *Proceedings of Machine Learning Research*, pages 531–540. PMLR, 07 2018.
- [6] A J Bell and T J Sejnowski. An information-maximization approach to blind separation and blind deconvolution. *Neural Comput.*, 7(6):1129–1159, November 1995.
- [7] Thomas Berrett and Richard Samworth. Nonparametric independence testing via mutual information. *Biometrika*, 106, 11 2017.
- [8] Thomas B. Berrett, Richard J. Samworth, and Ming Yuan. Efficient multivariate entropy estimation via  $k$ -nearest neighbour distances. *Ann. Statist.*, 47(1):288–318, 02 2019.
- [9] Valentin De Bortoli, Iryna Korshunova, Andriy Mnih, and Arnaud Doucet. Schrodinger bridge flow for unpaired data translation. In *The Thirty-eighth Annual Conference on Neural Information Processing Systems*, 2024.
- [10] Mustapha Bounoua, Giulio Franzese, and Pietro Michiardi.  $S_{\omega i}$ : Score-based o-INFORMATION estimation. In Ruslan Salakhutdinov, Zico Kolter, Katherine Heller, Adrian Weller, Nuria Oliver, Jonathan Scarlett, and Felix Berkenkamp, editors, *Proceedings of the 41st International Conference on Machine Learning*, volume 235 of *Proceedings of Machine Learning Research*, pages 4444–4471. PMLR, 21–27 Jul 2024.
- [11] Mustapha Bounoua, Giulio Franzese, and Pietro Michiardi.  $S_{\omega i}$ : Score-based o-information estimation. In *ICML 2024, 41st International Conference on Machine Learning*, 2024.
- [12] Charlotte Bunne, Ya-Ping Hsieh, Marco Cuturi, and Andreas Krause. The schrödinger bridge between gaussian measures has a closed form. In *International Conference on Artificial Intelligence and Statistics*, pages 5802–5833. PMLR, 2023.
- [13] Ivan Butakov, Alexander Tolmachev, Sofia Malanchuk, Anna Neopryatnaya, and Alexey Frolov. Mutual information estimation via normalizing flows. In *The Thirty-eighth Annual Conference on Neural Information Processing Systems*, 2024.

- [14] Ivan Butakov, Alexander Tolmachev, Sofia Malanchuk, Anna Neopryatnaya, Alexey Frolov, and Kirill Andreev. Information bottleneck analysis of deep neural networks via lossy compression. In *The Twelfth International Conference on Learning Representations*, 2024.
- [15] Xi Chen, Yan Duan, Rein Houthooft, John Schulman, Ilya Sutskever, and Pieter Abbeel. Infogan: Interpretable representation learning by information maximizing generative adversarial nets. In Daniel D. Lee, Masashi Sugiyama, Ulrike von Luxburg, Isabelle Guyon, and Roman Garnett, editors, *Advances in Neural Information Processing Systems 29: Annual Conference on Neural Information Processing Systems 2016, December 5-10, 2016, Barcelona, Spain*, pages 2172–2180, 2016.
- [16] Zehua Chen, Guande He, Kaiwen Zheng, Xu Tan, and Jun Zhu. Schrodinger bridges beat diffusion models on text-to-speech synthesis. *arXiv preprint arXiv:2312.03491*, 2023.
- [17] Thomas M. Cover and Joy A. Thomas. *Elements of Information Theory (Wiley Series in Telecommunications and Signal Processing)*. Wiley-Interscience, USA, 2006.
- [18] Paweł Czyż, Frederic Grabowski, Julia E Vogt, Niko Beerenwinkel, and Alexander Marx. Beyond normal: On the evaluation of mutual information estimators. In *Thirty-seventh Conference on Neural Information Processing Systems*, 2023.
- [19] Paweł Czyż, Frederic Grabowski, Julia E Vogt, Niko Beerenwinkel, and Alexander Marx. On the properties and estimation of pointwise mutual information profiles. *Transactions on Machine Learning Research*, 2025.
- [20] Caleb Dahlke and Jason Pacheco. Flow-based variational mutual information: Fast and flexible approximations. In *The Thirteenth International Conference on Learning Representations*.
- [21] Valentin De Bortoli, Guan-Horng Liu, Tianrong Chen, Evangelos A Theodorou, and Weillie Nie. Augmented bridge matching. *arXiv preprint arXiv:2311.06978*, 2023.
- [22] Giovanni Dosi and Andrea Roventini. More is different... and complex! the case for agent-based macroeconomics. *Journal of Evolutionary Economics*, 29:1–37, 2019.
- [23] Bao Duong and Thin Nguyen. Diffeomorphic information neural estimation. *Proceedings of the AAAI Conference on Artificial Intelligence*, 37(6):7468–7475, Jun. 2023.
- [24] Bao Duong and Thin Nguyen. Normalizing flows for conditional independence testing. *Knowledge and Information Systems*, 66, 08 2023.
- [25] Ahmed Elnaggar, Michael Heinzinger, Christian Dallago, Ghaliya Rehawi, Yu Wang, Llion Jones, Tom Gibbs, Tamas Feher, Christoph Angerer, Martin Steinegger, et al. Prottrans: towards cracking the language of life’s code through self-supervised learning. *IEEE Transactions on Pattern Analysis and Machine Intelligence*, 44:7112–7127, 2021.
- [26] Ammar Fayad and Majd Ibrahim. On slicing optimality for mutual information. In *Thirty-seventh Conference on Neural Information Processing Systems*, 2023.
- [27] Marco Federici, David Ruhe, and Patrick Forré. On the effectiveness of hybrid mutual information estimation, 2023.
- [28] Giulio Franzese, Mustapha BOUNOUA, and Pietro Michiardi. MINDE: Mutual information neural diffusion estimation. In *The Twelfth International Conference on Learning Representations*, 2024.
- [29] Z. Goldfeld, K. Greenewald, J. Niles-Weed, and Y. Polyanskiy. Convergence of smoothed empirical measures with applications to entropy estimation. *IEEE Transactions on Information Theory*, 66(7):4368–4391, 2020.
- [30] Ziv Goldfeld and Kristjan Greenewald. Sliced mutual information: A scalable measure of statistical dependence. In A. Beygelzimer, Y. Dauphin, P. Liang, and J. Wortman Vaughan, editors, *Advances in Neural Information Processing Systems*, 2021.

- [31] Ziv Goldfeld, Kristjan Greenewald, Theshani Nuradha, and Galen Reeves.  $\mathbb{H}$ -sliced mutual information: A quantitative study of scalability with dimension. In Alice H. Oh, Alekh Agarwal, Danielle Belgrave, and Kyunghyun Cho, editors, *Advances in Neural Information Processing Systems*, 2022.
- [32] Ziv Goldfeld, Ewout van den Berg, Kristjan H. Greenewald, Igor V. Melnyk, Nam H. Nguyen, Brian Kingsbury, and Yuri Polyanskiy. Estimating information flow in deep neural networks. In *ICML*, 2019.
- [33] Kristjan H. Greenewald, Brian Kingsbury, and Yuancheng Yu. High-dimensional smoothed entropy estimation via dimensionality reduction. In *IEEE International Symposium on Information Theory, ISIT 2023, Taipei, Taiwan, June 25-30, 2023*, pages 2613–2618. IEEE, 2023.
- [34] Nikita Gushchin, Sergei Kholkin, Evgeny Burnaev, and Alexander Korotin. Light and optimal schrödinger bridge matching. In *Forty-first International Conference on Machine Learning*, 2024.
- [35] Nikita Gushchin, Alexander Kolesov, Alexander Korotin, Dmitry Vetrov, and Evgeny Burnaev. Entropic neural optimal transport via diffusion processes. In *Advances in Neural Information Processing Systems*, 2023.
- [36] Nikita Gushchin, Daniil Selikhanovych, Sergei Kholkin, Evgeny Burnaev, and Alexander Korotin. Adversarial schrödinger bridge matching. *arXiv preprint arXiv:2405.14449*, 2024.
- [37] R Devon Hjelm, Alex Fedorov, Samuel Lavoie-Marchildon, Karan Grewal, Phil Bachman, Adam Trischler, and Yoshua Bengio. Learning deep representations by mutual information estimation and maximization. In *International Conference on Learning Representations*, 2019.
- [38] Jonathan Ho, Ajay Jain, and Pieter Abbeel. Denoising diffusion probabilistic models. *Advances in Neural Information Processing Systems*, 33:6840–6851, 2020.
- [39] Jonathan Ho and Tim Salimans. Classifier-free diffusion guidance. In *NeurIPS 2021 Workshop on Deep Generative Models and Downstream Applications*, 2021.
- [40] Jian Huang, Yuling Jiao, Lican Kang, Xu Liao, Jin Liu, and Yanyan Liu. Schrödinger-föllmer sampler. *IEEE Transactions on Information Theory*, 2024.
- [41] Oliver Ibe. *Markov processes for stochastic modeling*. Newnes, 2013.
- [42] Ilia Igashov, Arne Schneuing, Marwin Segler, Michael M Bronstein, and Bruno Correia. Retro-bridge: Modeling retrosynthesis with markov bridges. In *The Twelfth International Conference on Learning Representations*, 2024.
- [43] Bert Kappen. Lecture notes in cds machine learning, September 2024.
- [44] Beomsu Kim, Yu-Guan Hsieh, Michal Klein, Marco Cuturi, Jong Chul Ye, Bahjat Kavar, and James Thornton. Simple reflow: Improved techniques for fast flow models. In *The Thirteenth International Conference on Learning Representations*, 2025.
- [45] Diederik P. Kingma and Jimmy Ba. Adam: A method for stochastic optimization, 2017.
- [46] Durk P Kingma and Prafulla Dhariwal. Glow: Generative flow with invertible 1x1 convolutions. *Advances in neural information processing systems*, 31, 2018.
- [47] Peter E. Kloeden. *Numerical solution of stochastic differential equations / Peter E. Kloeden, Eckhard Platen*. Applications of mathematics; v. 23. Springer, Berlin, 1992.
- [48] Alexander Korotin, Nikita Gushchin, and Evgeny Burnaev. Light schrödinger bridge. In *The Twelfth International Conference on Learning Representations*.
- [49] L. F. Kozachenko and N. N. Leonenko. Sample estimate of the entropy of a random vector. *Problems Inform. Transmission*, 23:95–101, 1987.
- [50] Alexander Kraskov, Harald Stögbauer, and Peter Grassberger. Estimating mutual information. *Phys. Rev. E*, 69:066138, Jun 2004.

- [51] Kyungeun Lee and Wonjong Rhee. A benchmark suite for evaluating neural mutual information estimators on unstructured datasets. In *The Thirty-eight Conference on Neural Information Processing Systems Datasets and Benchmarks Track*.
- [52] Christian Léonard. A survey of the schrödinger problem and some of its connections with optimal transport. *arXiv preprint arXiv:1308.0215*, 2013.
- [53] Christian Léonard. Some properties of path measures. *Séminaire de Probabilités XLVI*, pages 207–230, 2014.
- [54] Christian Léonard, Sylvie Røelly, and Jean-Claude Zambrini. Reciprocal processes. a measure-theoretical point of view. *Probability Surveys*, 11:237–269, 2014.
- [55] R. Linsker. Self-organization in a perceptual network. *Computer*, 21(3):105–117, 1988.
- [56] Guan-Horng Liu, Arash Vahdat, De-An Huang, Evangelos A Theodorou, Weili Nie, and Anima Anandkumar. I<sup>2</sup>sb: Image-to-image schrödinger bridge. *arXiv preprint arXiv:2302.05872*, 2023.
- [57] David McAllester and Karl Stratos. Formal limitations on the measurement of mutual information. In Silvia Chiappa and Roberto Calandra, editors, *Proceedings of the Twenty Third International Conference on Artificial Intelligence and Statistics*, volume 108 of *Proceedings of Machine Learning Research*, pages 875–884. PMLR, 08 2020.
- [58] Bernt Øksendal. *Stochastic differential equations*. Springer, 2003.
- [59] Zbigniew Palmowski and Tomasz Rolski. A technique for exponential change of measure for markov processes. *Bernoulli*, pages 767–785, 2002.
- [60] Stefano Peluchetti. Diffusion bridge mixture transports, schrödinger bridge problems and generative modeling. *Journal of Machine Learning Research*, 24(374):1–51, 2023.
- [61] Y. Polyanskiy and Y. Wu. *Information Theory: From Coding to Learning*. Cambridge University Press, 2024.
- [62] Benjamin Rhodes, Kai Xu, and Michael U. Gutmann. Telescoping density-ratio estimation. In H. Larochelle, M. Ranzato, R. Hadsell, M.F. Balcan, and H. Lin, editors, *Advances in Neural Information Processing Systems*, volume 33, pages 4905–4916. Curran Associates, Inc., 2020.
- [63] Robin Rombach, Andreas Blattmann, Dominik Lorenz, Patrick Esser, and Björn Ommer. High-resolution image synthesis with latent diffusion models. In *Proceedings of the IEEE/CVF Conference on Computer Vision and Pattern Recognition*, pages 10684–10695, 2022.
- [64] Olaf Ronneberger, Philipp Fischer, and Thomas Brox. U-net: Convolutional networks for biomedical image segmentation. In *Medical image computing and computer-assisted intervention—MICCAI 2015: 18th international conference, Munich, Germany, October 5-9, 2015, proceedings, part III 18*, pages 234–241. Springer, 2015.
- [65] Fernando E Rosas, Pedro AM Mediano, Michael Gastpar, and Henrik J Jensen. Quantifying high-order interdependencies via multivariate extensions of the mutual information. *Physical Review E*, 100(3):032305, 2019.
- [66] Jakob Runge, Sebastian Bathiany, Erik Bollt, Gustau Camps-Valls, Dim Coumou, Ethan Deyle, Clark Glymour, Marlene Kretschmer, Miguel D Mahecha, Jordi Muñoz-Marí, et al. Inferring causation from time series in earth system sciences. *Nature communications*, 10(1):2553, 2019.
- [67] Erwin Schrödinger. Sur la théorie relativiste de l’électron et l’interprétation de la mécanique quantique. In *Annales de l’institut Henri Poincaré*, volume 2, pages 269–310, 1932.
- [68] Rajat Sen, Ananda Theertha Suresh, Karthikeyan Shanmugam, Alexandros G Dimakis, and Sanjay Shakkottai. Model-powered conditional independence test. In I. Guyon, U. Von Luxburg, S. Bengio, H. Wallach, R. Fergus, S. Vishwanathan, and R. Garnett, editors, *Advances in Neural Information Processing Systems*, volume 30. Curran Associates, Inc., 2017.

- [69] Yuyang Shi, Valentin De Bortoli, Andrew Campbell, and Arnaud Doucet. Diffusion schrödinger bridge matching. In *Thirty-seventh Conference on Neural Information Processing Systems*, 2023.
- [70] Vignesh Ram Somnath, Matteo Pariset, Ya-Ping Hsieh, Maria Rodriguez Martinez, Andreas Krause, and Charlotte Bunne. Aligned diffusion schrödinger bridges. In *Uncertainty in Artificial Intelligence*, pages 1985–1995. PMLR, 2023.
- [71] Jiaming Song and Stefano Ermon. Understanding the limitations of variational mutual information estimators. In *International Conference on Learning Representations*, 2020.
- [72] Yang Song, Jascha Sohl-Dickstein, Diederik P Kingma, Abhishek Kumar, Stefano Ermon, and Ben Poole. Score-based generative modeling through stochastic differential equations. In *International Conference on Learning Representations*, 2021.
- [73] Thomas Steinke and Lydia Zakyntinou. Reasoning About Generalization via Conditional Mutual Information. In Jacob Abernethy and Shivani Agarwal, editors, *Proceedings of Thirty Third Conference on Learning Theory*, volume 125 of *Proceedings of Machine Learning Research*, pages 3437–3452. PMLR, 09–12 Jul 2020.
- [74] Vincent Stimper, David Liu, Andrew Campbell, Vincent Berenz, Lukas Ryll, Bernhard Schölkopf, and José Miguel Hernández-Lobato. normflows: A pytorch package for normalizing flows. *Journal of Open Source Software*, 8(86):5361, 2023.
- [75] Karl Stratos. Mutual information maximization for simple and accurate part-of-speech induction. In Jill Burstein, Christy Doran, and Thamar Solorio, editors, *Proceedings of the 2019 Conference of the North American Chapter of the Association for Computational Linguistics: Human Language Technologies, Volume 1 (Long and Short Papers)*, pages 1095–1104, Minneapolis, Minnesota, June 2019. Association for Computational Linguistics.
- [76] Naftali Tishby and Noga Zaslavsky. Deep learning and the information bottleneck principle. *2015 IEEE Information Theory Workshop (ITW)*, pages 1–5, 2015.
- [77] Alexander Y Tong, Nikolay Malkin, Kilian Fatras, Lazar Atanackovic, Yanlei Zhang, Guillaume Huguët, Guy Wolf, and Yoshua Bengio. Simulation-free schrödinger bridges via score and flow matching. In *International Conference on Artificial Intelligence and Statistics*, pages 1279–1287. PMLR, 2024.
- [78] Michael Tschannen, Josip Djolonga, Paul K. Rubenstein, Sylvain Gelly, and Mario Lucic. On mutual information maximization for representation learning. In *International Conference on Learning Representations*, 2020.
- [79] Dor Tsur, Ziv Goldfeld, and Kristjan Greenewald. Max-sliced mutual information. In *Thirty-seventh Conference on Neural Information Processing Systems*, 2023.
- [80] Aaron van den Oord, Yazhe Li, and Oriol Vinyals. Representation learning with contrastive predictive coding, 2019.
- [81] Francisco Vargas, Andrius Ovsianas, David Fernandes, Mark Girolami, Neil D Lawrence, and Nikolas Nüsken. Bayesian learning via neural schrödinger–föllmer flows. *Statistics and Computing*, 33(1):3, 2023.
- [82] Francisco Vargas, Pierre Thodoroff, Austen Lamacraft, and Neil Lawrence. Solving schrödinger bridges via maximum likelihood. *Entropy*, 23(9):1134, 2021.
- [83] Petar Veličković, William Fedus, William L. Hamilton, Pietro Liò, Yoshua Bengio, and R Devon Hjelm. Deep graph infomax. In *International Conference on Learning Representations*, 2019.
- [84] Chao Wang, Giulio Franzese, Alessandro Finamore, Massimo Gallo, and Pietro Michiardi. Information theoretic text-to-image alignment, 2024.
- [85] Stanislaw Węglarczyk. Kernel density estimation and its application. *ITM Web of Conferences*, 23:00037, 01 2018.

- [86] Aolin Xu and Maxim Raginsky. Information-theoretic analysis of generalization capability of learning algorithms. *Advances in neural information processing systems*, 30, 2017.
- [87] Eun Bi Yoon, Keehun Park, Sungwoong Kim, and Sungbin Lim. Score-based generative models with lévy processes. *Advances in Neural Information Processing Systems*, 36:40694–40707, 2023.
- [88] Linqi Zhou, Aaron Lou, Samar Khanna, and Stefano Ermon. Denoising diffusion bridge models. In *The Twelfth International Conference on Learning Representations*, 2024.

## A Limitations

Our approach is based on the diffusion bridge matching framework [60, 69]. While this class of models and its theoretical foundations have demonstrated strong potential in high-dimensional generative modeling [69, 56, 72], they also have certain limitations that, while often negligible in the context of generative modeling, can be more pronounced in other applications.

One such limitation, evident in our work, is the challenge of accurately approximating heavy-tailed distributions. As can be seen in Table 1, one-degree-of-freedom Student-t distribution, i.e.,  $St(\text{dof}=1)$ , also known as Cauchy distribution, has no first moment, and our method is not guaranteed to work in such a case due to theoretical requirements of bridge matching [69, Appendix C]. However, it is worth noting that such limitations are quite common for generative modeling and quite probably should be applicable to denoising score matching and diffusion models as well [28, 72]. Another limitation of diffusion (and diffusion bridge matching) is that it requires a lot of data samples at training stage. This could hinder the applicability of our method with low number of data samples.

## B Extensions of our methodology

In this appendix section we present:

- Appendix B.1. General KL divergence estimation method with proof and discussion.
- Appendix B.2. Differential entropy estimation result with two possible algorithms and discussion.
- Appendix B.3. Experimental illustrations to the entropy estimation algorithm.
- Appendix B.4. Interaction information estimation method.

### B.1 KL divergence estimator

In this section, we present a general result for the unbiased estimation of KL divergence between any two distributions  $\pi_1(x), \pi_2(x) \in \mathcal{P}(\mathbb{R}^d)$  through the difference of drifts in the SDE formulation (4) of reciprocal processes induced by these distributions, i.e.:

$$Q_{\pi_1} \stackrel{\text{def}}{=} \int W_{|x_0, x_1}^\epsilon d\pi_1(x_1) dp(x_0), \quad (14)$$

$$Q_{\pi_2} \stackrel{\text{def}}{=} \int W_{|x_0, x_1}^\epsilon d\pi_2(x_1) dp(x_0). \quad (15)$$

**Theorem B.1** (KL divergence decomposition). *Consider distributions  $\pi_1(x_1), \pi_2(x_1), p(x_0) \in \mathcal{P}(\mathbb{R}^d)$ , that satisfy some regularity assumptions [69, Appendix C], and reciprocal processes  $Q_{\pi_1}, Q_{\pi_2}$  induced by distributions  $\pi_1(x_1), \pi_2(x_1)$  (14), (15). Then the KL divergence between distributions  $\pi_1(x_1)$  and  $\pi_2(x_1)$  can be represented in the following way:*

$$\text{KL}(\pi_1(x_1) \parallel \pi_2(x_1)) = \frac{1}{2\epsilon} \int_0^1 \mathbb{E}_{q_{\pi_1}(x_t, x_0)} [\|v^{\pi_1}(x_t, t, x_0) - v^{\pi_2}(x_t, t, x_0)\|^2] dt, \quad (16)$$

where

$$v^{\pi_1}(x_t, t, x_0) = \mathbb{E}_{q_{\pi_1}(x_1 | x_t, x_0)} \left[ \frac{x_1 - x_t}{1 - t} \right], \quad (17)$$

$$v^{\pi_2}(x_t, t, x_0) = \mathbb{E}_{q_{\pi_2}(x_1 | x_t, x_0)} \left[ \frac{x_1 - x_t}{1 - t} \right] \quad (18)$$

are the drifts of reciprocal processes  $Q_{\pi_1}$  and  $Q_{\pi_2}$  respectively. Holds for any distribution  $p(x_0)$ .

Our theorem allows us to estimate  $\text{KL}(\pi_1(x) \parallel \pi_2(x))$  knowing only the drifts  $v^{\pi_1}(x_t, t, x_0)$  and  $v^{\pi_2}(x_t, t, x_0)$ , which can be recovered using conditional bridge matching §2. Note that the expression (16) is very similar to the expression (10) in §4.1. Distribution  $p(x_0)$ , can be considered as part of the design space and optimised for each particular problem.

The KL divergence is a fundamental quantity, and its estimator can have many applications, such as mutual information estimation or entropy estimation using results described in Appendix B.2.



*Proof.* Consider

$$\begin{aligned} \text{KL}(\pi_1(x_1)p(x_0)\|\pi_2(x_1)p(x_0)) &= \underbrace{\text{KL}(p(x_0)\|p(x_0))}_{=0} + \mathbb{E}_{p(x_0)} [\text{KL}(\pi_1(x_1|x_0)\|\pi_2(x_1|x_0))] = \\ &= \mathbb{E}_{p(x_0)} [\text{KL}(\pi_1(x_1)\|\pi_2(x_1))] = \text{KL}(\pi_1(x_1)\|\pi_2(x_1)), \end{aligned}$$

Next to get

$$\text{KL}(\pi_1(x_1)p(x_0)\|\pi_2(x_1)p(x_0)) = \frac{1}{2\epsilon} \int_0^1 \mathbb{E}_{q_{\pi_1}(x_t, x_0)} [\|v^{\pi_1}(x_t, t, x_0) - v^{\pi_2}(x_t, t, x_0)\|^2] dt,$$

one can repeat all the steps that were taken to show:

$$\text{KL}(\pi(x_0, x_1)\|\pi(x_0)\pi(x_1)) = \frac{1}{2\epsilon} \int_0^1 \mathbb{E}_{q_{\pi}(x_t, x_0)} [\|v_{\text{joint}}(x_t, t, x_0) - v_{\text{ind}}(x_t, t, x_0)\|^2] dt,$$

in the proof of Theorem 4.1. □

## B.2 Differential entropy estimator

A general result on the information projections and maximum-entropy distributions suggests a way of calculating differential entropy through the KL divergence estimation.

**Theorem B.2** (Theorem 6.7 in [43]). *Let  $\phi: \mathbb{R}^n \rightarrow \mathbb{R}^k$  be any measurable function, an absolutely continuous probability distribution  $p(x) \in \mathcal{P}(\mathbb{R}^d)$  and define  $\alpha \stackrel{\text{def}}{=} \mathbb{E}_p \phi(x)$ . Now, for any  $\theta \in \mathbb{R}^k$  consider an absolutely continuous probability distribution  $q_\theta \in \mathcal{P}(\mathbb{R}^d)$  with density:*

$$q_\theta(x) = \exp(\langle \theta, \phi(x) \rangle - A(\theta)), \quad A(\theta) = \log \mathbb{E}_{q_\theta(x)} e^{\langle \theta, \phi(x) \rangle}.$$

*If there exists  $\theta^*$  such that  $p$  is absolutely continuous w.r.t.  $q_{\theta^*}$  and  $\mathbb{E}_{q_{\theta^*}(x)} \phi(x) = \alpha$ , then*

$$H(p) = H(q_{\theta^*}) - \text{KL}(p\|q_{\theta^*}),$$

**Corollary B.3.** *Let  $X$  be a  $d$ -dimensional absolutely continuous random vector with probability density function  $p$ , mean  $m$  and covariance matrix  $\Sigma$ . Then*

$$H(p) = H(\mathcal{N}(m, \Sigma)) - \text{KL}(p\|\mathcal{N}(m, \Sigma)), \quad H(\mathcal{N}(m, \Sigma)) = \frac{1}{2} \log((2\pi e)^d \det \Sigma),$$

where  $\mathcal{N}(m, \Sigma)$  is a Gaussian distribution of mean  $m$  and covariance matrix  $\Sigma$ .

**Corollary B.4.** *Let  $X$  be an absolutely continuous random vector with probability density function  $p$  and  $\text{supp } X = S$ , where  $S$  has finite and non-zero Lebesgue measure  $\mu(S)$ . Then*

$$H(p) = H(\text{U}(S)) - \text{KL}(p\|\text{U}(S)), \quad H(\text{U}(S)) = \log \mu(S),$$

where  $\text{U}(S)$  is a uniform distribution on  $S$ .

Similar results can also be obtained for other members of the exponential family. The first result (Corollary B.3) can be considered as a general recipe, while the second one (Corollary B.4) can be useful when we have prior knowledge about the support of  $X$  being restricted. Approach described in Theorem B.2 is very flexible and can be considered as a generalization of the method used in [28].

In practice, to estimate the entropy of some probability distribution, it is sufficient to follow one of the described in Corollaries B.3 and B.4. For example, if one uses Corollary B.3: 1) estimate mean  $m$  and covariance matrix  $\Sigma$  using a set of data samples, 2) calculate entropy  $H(\mathcal{N}(m, \Sigma))$  via the closed form expression, 3) calculate the KL divergence  $\text{KL}(p\|\mathcal{N}(m, \Sigma))$  via learning two conditional diffusion bridges models and utilizing our estimator (16) from Theorem B.1.

### B.3 Entropy estimation experiments

We conduct entropy estimation experiments using our method proposed in Appendix B.2. We estimate the entropy of high-dimensional ( $D = 10$ ) exponential and uniform distributions  $\pi$  with varying distribution parameters. Corollary B.3 (Gaussian) method is used for the both distributions and Corollary B.4 (Uniform) method for the uniform distribution, since it has finite support. For each of the setups we prepare the dataset of 8000 training and 2000 test samples. Additionally we explore different reference distributions  $p(x_0)$ , see Theorem B.1, for the  $\text{KL}(\cdot \| \mathcal{N}(m, \Sigma))$  or  $\text{KL}(\cdot \| U(S))$  estimation. We explored four reference distributions  $p(x_0)$ ,: low ( $\epsilon = 0.1$ ), medium ( $\epsilon = 1$ ), and high ( $\epsilon = 10$ ) variance Gaussians (all with zero mean), and a "data Gaussian" with mean and standard deviation derived from the training data.

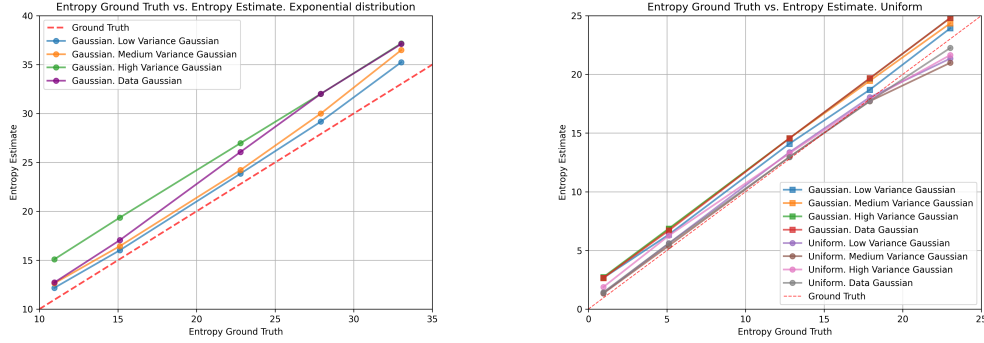


Figure 3: Comparison of our *InfoBridge* combined with different methods Corollary B.3 (Gaussian) and Corollary B.4 (Uniform) and with different reference distributions  $p(x_0)$  on the entropy estimation task. Along  $x$  axes is the ground truth entropy  $H(X)$ , along  $y$  axes is the entropy estimate  $\hat{H}(X)$ . Each configuration is ran once.

One can observe that *InfoBridge* is capable of entropy estimation on practice. Versions with low/medium variance gaussians generally show superior performance to high variance gaussian and data gaussian. In the case of uniform distribution (Corollary B.4) method performs a lot better, suggesting that it is preferable in the cases when it can be applied (restricted support distributions).

### B.4 Interaction information

Here we propose the generalization of *InfoBridge* for the *interaction information* estimation, which is the generalization of mutual information for more than two random variables [65]. Interaction information for random variables  $X_0, X_1, X_2$  is defined by:

$$\begin{aligned} I(X_0; X_1; X_2) &\stackrel{\text{def}}{=} I(X_0; X_1) - I(X_0; X_1 | X_2) = \\ &= \text{KL}(\Pi_{X_0, X_1} \| \Pi_{X_0} \otimes \Pi_{X_1}) - \text{KL}(\Pi_{X_0, X_1 | X_2} \| \Pi_{X_0 | X_2} \otimes \Pi_{X_1 | X_2}). \end{aligned} \quad (19)$$

This definition can be generalized for more random variables in a similar way. Both MI information terms can be estimated using Theorem 4.1 and our practical algorithm *InfoBridge*. Applications of interaction information include neuroscience [11], climate models [66], econometrics [22].

## C Experimental supplementary

In this section, additional experimental results and experimental details are described.

### C.1 Ablation study

**InfoBridge ablation study** Here we vary different important hyperparameters of our *InfoBridge* method.

**Volatility coefficient  $\epsilon$ .** We evaluate different volatility coefficients on the image benchmark §5.2 and protein embeddings data §5.3. We run the image benchmark experiment on Gaussian 16x16 setting with ground truth MI=10 and the full protein embeddings data experiment with one random seed and report mean MAE error for the last 5 measurements during training, in both of setups. Results are presented in Table 2 and Table 3. One can see that MAE relatively stable for all the setups, while the optimal  $\epsilon$  values is different for the both experiments. However, one can notice that  $\epsilon = 1$  works relatively well on both of the setups and can be called a robust choice. For consistency we use  $\epsilon = 1$  for the experiments in the main part of the paper, despite it may be not optimal for each data type separately.

Table 2: Mean Average Error (MAE) values on Image data benchmark (Gaussian 16x16) with ground truth MI=10 experiment for the different  $\epsilon$  values. Each configuration (except for  $\epsilon = 1$ ) is ran one time and 5 last MI measurements during training are averaged to produce the shown result. The best configuration is **bolded** and configuration used in the main part of the paper is underlined.

$\epsilon$	0.001	0.003	0.01	0.03	0.1	0.3	1	3	10
MAE ↓	2.09	1.79	<b>1.53</b>	<b>1.53</b>	1.72	1.79	<u>2.46</u>	2.82	6.45

Table 3: Mean Average Error (MAE) values on ProtTran5 experiment, averaged over all the ground truth MI values, for the different  $\epsilon$  values. Each configuration (except for  $\epsilon = 1$ ) is ran one time and 5 last MI measurements during training are averaged to produce the shown result. The best configuration is **bolded** and configuration used in the main part of the paper is underlined.

$\epsilon$	0.1	0.3	1	3	10
MAE ↓	0.775	0.232	<b>0.04</b>	0.089	0.129

**Number of parameters in a neural network.** The width of the Unet [64] neural network architecture used in *InfoBridge* on Image benchmark experiments is varied to yield different number of parameters of a neural network. Numbers of base filters, 256, 64, 32, 16, 8, yield number of parameters, 27M, 1.7M, 428K, 108k, 28k. Similar to the ablation study on  $\epsilon$  each configuration, except for 256 number of filters and 27M parameters is run once, and the final five mutual information (MI) measurements during training are averaged to obtain the reported results. Outcomes are presented in Table 4. As one can see our *InfoBridge* is robust w.r.t. neural network architecture.

Table 4: Comparison of the *InfoBridge* with different neural network architectures on the Image data benchmark (16 × 16 Gaussians setup) with ground truth MI=7.5. Each configuration is ran one time and 5 last MI measurements during training are averaged to produce the shown result. The configuration used in the main experimental part is underlined.

N Params	GT MI=7.5 (mean ± std)
28k	7.56 ± 0.3
108k	6.67 ± 0.15
428k	6.67 ± 0.13
1.7M	6.52 ± 0.07
<u>27M</u>	6.59 ± 0.17

## C.2 Low-dimensional benchmark

**Additional results.** In the Table 9 we present the results of low-dimensional benchmark [18] with precision of 0.01 nats.

**Experimental details.** The benchmark implementation was taken from the official repository:

<https://github.com/cbg-ethz/bmi>

Table 5: Neural networks hyperparameters for low-dimensional [18] benchmark. “Dim” - dimensionality of a MI estimation problem, “Filters” – number of filters in MLP, “Time Embed” – number of filters in time embedding module, “Parameters” – number of overall neural networks parameters.

Dim	Filters	Time Embed	Parameters
$\leq 5$	64	64	43K
25	128	128	176K
50	256	256	699K

**InfoBridge.** Neural networks were taken of almost the same architecture as in [28], which is MLP with residual connections and time embedding. Additional input  $s$  described in § 4.2 was processed the same way as time input. Number of parameters was taken depending on a dimensionality of the problem, see Table 5. Exponential Moving Average as a widely recognized training stabilization method was used with decay parameter of 0.999. For all the problems neural networks were trained during 100k iterations with  $\epsilon = 1$ , batch size 512, lr 0.0003. Mutual Information was estimated by Algorithm 2 with  $N$  pairs of samples  $\{x_t^i, x_0^i, t^i\}_{i=1}^N$ , where  $N$  is equal to the number of test samples times 10, i.e., 100k.

**NVF and JVF.** The implementation of NVF and JVF was taken from the official repository:

<https://github.com/calebdahlke/FlowMI>

and used with all the provided by authors default hyperparameters for the benchmark. The methods were ran on CPU and execution took less then two hours for each benchmark problem run.

### C.3 Image data benchmark

Table 6: Mean Average Error (MAE) and mean std across random seeds for each method presented for comparison in Sec 5.2. The best result is **bolded and underlined** and second best result is **bolded**. Inductive bias stands for matching intrinsic dimensionality, Appendix C.5.

Method	InfoBridge (ours)	AE+WKL (inductive bias, d=2)	AE+WKL (d=5)	KSG	MINE	MIENF	NWJ	MINDE-C	MINDE-J
MAE ↓	<b>0.38</b>	<b>0.26</b>	1.22	1.15	0.92	0.45	1.24	0.56	1.66
Average Std	0.07	0.06	0.07	0.02	0.13	0.08	0.08	0.43	0.45

**Experimental details for InfoBridge.** The implementation of image data benchmark [13] was taken from the official repository:

<https://github.com/VanessB/mutinfo>

Following authors of the benchmark, *Gaussian* images were generated with all the default settings, *Rectangle* images were also generated with all the default settings, but minimum size of rectangle is 0.2 to avoid singularities. All the covariance matrices for the distributions defining the mutual information in the benchmark were generated without randomization of component-wise mutual information, but with randomization of the off-diagonal blocks of the covariance matrix.

To approximate the drift coefficient of diffusion U-Net [64] with time, conditional neural networks were used, special input  $s$  was processed as time input. For all the tests, neural networks were the same and had 2 residual layers per U-net block with 256 base channels, positional timestep encoding, upscale and downscale blocks consisting of two resnet blocks, one with attention and one without attention. The number of parameters is  $\sim 27$ M. During the training, 100k gradient steps were made with batch size of 64 and learning rate 0.0001. Exponential moving average was used with decay rate 0.999. Mutual Information was estimated by Algorithm 2 with  $N$  pairs of samples  $\{x_t^n, x_0^n, t^n\}_{i=n}^N$ , where  $N$  is equal to the number of test samples, i.e., 10k. Nvidia A100 was used for the *InfoBridge* training. Each run (one seed) took around 6 and 18 GPU-hours for the  $16 \times 16$  and  $32 \times 32$  image resolution setups, respectively.

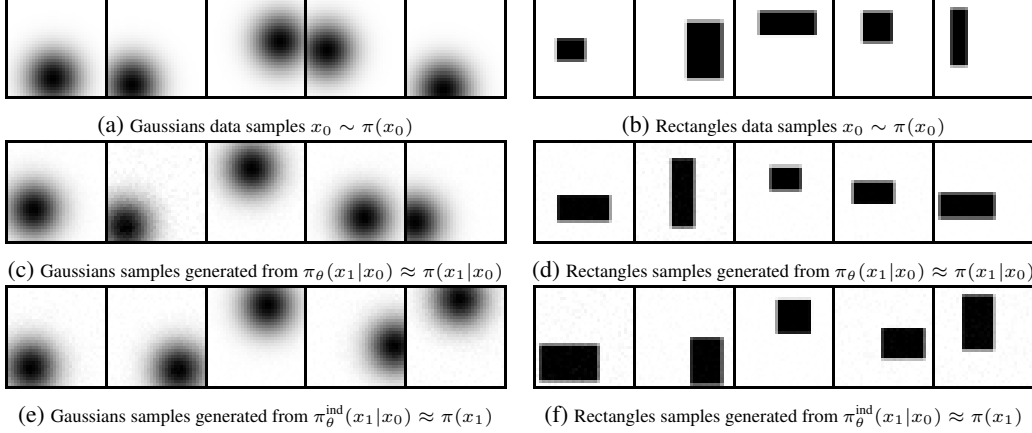


Figure 4: Examples of synthetic images from the [13] benchmark can be seen in Figures 4a and 4b. Note that images are high-dimensional, but admit latent structure, which is similar to real datasets. Samples generated by our *InfoBridge* from the learned distributions  $\pi_\theta(x_1|x_0) \approx \pi(x_1|x_0)$  and  $\pi_\theta^{\text{ind}}(x_1|x_0) \approx \pi(x_1)$  defined as solutions to SDEs (4) with approximated drifts  $v_\theta(\cdot, 0)$  and  $v_\theta(\cdot, 1)$ , respectively, can be seen at Figures 4c to 4f. All the images have  $32 \times 32$  resolution.

**Visualization of learned distribution.** Figure 4 presents samples generated from the learned distributions alongside ground truth samples from the dataset. It is evident that the samples from both  $\pi_\theta(x_1|x_0)$  and  $\pi_\theta^{\text{ind}}(x_1|x_0)$  closely resemble those drawn from  $\pi(x_0)$ , indicating that the marginal distribution of  $x_0$  is well approximated by the learned models.

**Experimental details for other methods.** In this part, we provide additional experimental details regarding other methods featured in Figure 1. We report the NN architectures used for neural estimators in Table 7.

Table 7: The NN architectures used to conduct the tests with images in Section 5.

NN	Architecture	
GLOW, $16 \times 16 (32 \times 32)$ images	$\times 1$ :	4 (5) splits, 2 GLOW blocks between splits, $\times 2$ in parallel
	$\times 1$ :	16 hidden channels in each block, leaky constant = 0.01
Autoencoder, $16 \times 16 (32 \times 32)$ images	$\times 1$ :	Conv2d(1, 4, ks=3), BatchNorm2d, LeakyReLU(0.2), MaxPool2d(2)
	$\times 1$ :	Conv2d(4, 8, ks=3), BatchNorm2d, LeakyReLU(0.2), MaxPool2d(2)
	$\times 2(3)$ :	Conv2d(8, 8, ks=3), BatchNorm2d, LeakyReLU(0.2), MaxPool2d(2)
	$\times 1$ :	Dense(8, dim), Tanh, Dense(dim, 8), LeakyReLU(0.2)
	$\times 3(4)$ :	Upsample(2), Conv2d(8, 8, ks=3), BatchNorm2d, LeakyReLU(0.2)
Critic NN, $16 \times 16 (32 \times 32)$ images	$\times 1$ :	Upsample(2), Conv2d(8, 4, ks=3), BatchNorm2d, LeakyReLU(0.2)
	$\times 1$ :	Conv2d(4, 1, ks=3), BatchNorm2d, LeakyReLU(0.2)
	$\times 1$ :	[Conv2d(1, 16, ks=3), MaxPool2d(2), LeakyReLU(0.01)] $\times 2$ in parallel
	$\times 1(2)$ :	[Conv2d(16, 16, ks=3), MaxPool2d(2), LeakyReLU(0.01)] $\times 2$ in parallel
	$\times 1$ :	Dense(256, 128), LeakyReLU(0.01)
	$\times 1$ :	Dense(128, 128), LeakyReLU(0.01)
	$\times 1$ :	Dense(128, 1)

**MINDE.** We use the official implementation of MINDE:

<https://github.com/MustaphaBounoua/minde>

As a neural network, we adapt same U-net architecture as for our *InfoBridge* in image data experiments with approximately the same number of parameters. Training procedure hyperparameters do match the *InfoBridge*, i.e., 100k gradient steps with batch size 64 and learning rate 0.0001, exponential

moving average with 0.999 decay rate. Mutual Information was estimated using 10 samples of  $\{t^i, x_t^i\}$  per each pair  $\{x_0^i, x_1^i\}$  in the test dataset. Nvidia A100 was used to train the models. Each run (one seed) took around 2 and 5 GPU-hours for the  $16 \times 16$  and  $32 \times 32$  image resolution setups.

**MIENF.** This method is based on bi-gaussianization of the input data via a Cartesian product of learnable diffeomorphisms [13]. Such approach allows for a closed-form expression to be employed to estimate the MI.

With only minor stability-increasing changes introduced, we adopt the Glow [46] flow network architecture from [13], which is also reported in Table 7 (“GLOW”). We used the `normflows` package [74] to implement the model. Adam [45] optimizer was used to train the network on  $10^5$  images with a batch size 512, and the learning rate decreasing from  $5 \cdot 10^{-4}$  to  $10^{-5}$  geometrically. For averaging, we used 3 different seeds. Nvidia A100 was used to train the flow models. Each run (one seed) took no longer than four GPU-hours to be completed.

**KSG.** Kraskov-Stögbauer-Grassberger [50] mutual information estimator is a well-known  $k$ -NN non-parametric method, which is very similar to unweighted Kozachenko-Leonenko estimator [49]. This method employs distances to  $k$ -th nearest neighbors to approximate the pointwise mutual information, which is then averaged.

We used  $k = 1$  (one nearest neighbour) for all the tests. The number of samples was  $10^5$  for Gaussian images and  $10^4$  for images of rectangles (we had to lower the sampling size due to degenerated performance of the metric tree-based  $k$ -NN search in this particular setup). A single core of AMD EPYC 7543 CPU was used for nearest neighbors search and MI calculation. Each run (one seed) took no longer than one CPU-hour to be completed.

**AE+WKL 5-NN.** The idea of leveraging lossy compression to tackle the curse of dimensionality and provide better MI estimates is well-explored in the literature [30, 31, 79, 26, 33, 14]. In our work, we adopt the non-linear compression setup from [14], which employs autoencoders for data compression and weighted Kozachenko-Leonenko method [8] for MI estimation in the latent space.

The autoencoders were trained using Adam optimizer on  $10^5$  images with a batch size 512, a learning rate  $10^{-3}$  and MAE loss for  $10^4$  steps. For averaging, we used 5 different seeds. Nvidia A100 was used to train the autoencoder model. Each run (one seed) took no longer than one GPU-hour to be completed.

**MINE, NWJ, InfoNCE.** These discriminative approaches are fundamentally alike: each method estimates mutual information by maximizing the associated KL-divergence bound:

$$I(X_0; X_1) = \text{KL}(\pi(x_0, x_1) \| \pi(x_0)\pi(x_1)) \geq \sup_{T: \mathbb{R}^d \times \mathbb{R}^d \rightarrow \mathbb{R}} \mathbb{E}[T(x_0, x_1)], \quad (20)$$

where  $T$  is measurable, and  $\mathbb{E}$  is some method-specific functional. In practice,  $T$  is approximated via a neural network, with the right-hand-side in (20) being used as the loss function.

Motivated by this similarity, we use a nearly identical experimental framework to assess each approach within this category. To approximate  $T$  in experiments with synthetic images, we adopt the critic NN architecture from [13], which we also report in Table 7 (“Critic NN”).

The networks were trained via Adam optimizer on  $10^5$  images with a learning rate  $10^{-3}$ , a batch size 512 (with InfoNCE being the only exception, for which we used batch size 256 for training and 512 for evaluation due to memory constraints), and MAE loss for  $10^5$  steps. For averaging, we used 5 different seeds. Nvidia A100 was used to train the models. In any setup, each run (one seed) took no longer than two GPU-hours to be completed.

#### C.4 Protein embeddings data

Table 8: The best result is **bolded and underlined** and second best result is **bolded**.

Method	<i>InfoBridge</i>	MINE	InfoNCE	KSG	MINDE-C	MINDE-J
MAE ↓	<b><u>0.04</u></b>	0.223	0.237	<b>0.116</b>	9.29	1342
MAE Std	0.01	0.017	0.007	-	1.1	57

**Data.** We use the UniProt database proteins, their embeddings from prottrans\_t5\_xl\_u50 [25] model and download them from <https://github.com/ggdna/latent-mutual-information>. All proteins longer than  $12 \cdot 10^3$  residues are excluded. These embeddings are then unit variance normalized. The final number of each protein embeddings (samples) used for training is 20641 and the dimensionality is 1024.

#### Methods implementation.

**InfoBridge.** Hyperparameters are the same as for low-dimensional benchmark Appendix C.2, MLP has  $\sim 900k$  parameters, weight decay is 0.001, dropout is 0.2 and the model is trained for 100 epochs.

**MINDE.** We leverage the official implementation of MINDE <https://github.com/MustaphaBounoua/minde> in the configuration used for the low-dimensional benchmark, with  $\sim 900k$  parameters MLP, lr  $1e-4$ , batch size of 256, ema decay of 0.999 and train model for 100 epochs.

**MINE, InfoNCE.** These estimators are taken from the *bmi* library <https://github.com/cbg-ethz/bmi> with all the default parameters.

**KSG.** Implementation is taken from <https://github.com/ggdna/latent-mutual-information> and used with all the default parameters on 20000 training samples.

All the neural methods were trained on Nvidia A100 and took less than one GPU-hour to complete. KSG estimation algorithm took approximately one hour to complete.

#### C.5 Additional experiments with AE+WKL estimator using higher bottleneck dimensionality

Prior works suggest that non-parametric MI estimators are highly prone to the curse of dimensionality compared to NN-based approaches [29, 18, 13]. In particular, Figures 2 and 3 in [29] and Table 1 in [13] indicate that weighted Kozachenko-Leonenko estimator fails to yield reasonable estimates at all if the dimensionality reaches certain threshold. That is why autoencoders are used in our setup to acquire MI estimates for high-dimensional synthetic images.

However, this approach introduces a substantial inductive bias. Not only we assume the data to be distributed on a manifold, but also select the bottleneck dimensionality of the autoencoders to be equal to the ground-truth intrinsic dimensionality, which is usually not available in practical scenarios. Such prior knowledge allows for remarkable results, as it can be seen in Figure 1. However, we argue that even slight changes to this experimental protocol can lead to severe problems. In the Gaussian images setup, increasing the bottleneck dimensionality from  $d = 2$  (which is the intrinsic dimensionality of the dataset in question) to  $d \in \{4, 5, 8\}$  completely destabilizes the estimator, with  $d = 8$  even leading to exploded estimates. We report our results in Figure 5; all the other details of the experimental setup are identical to the settings used for Figure 1.

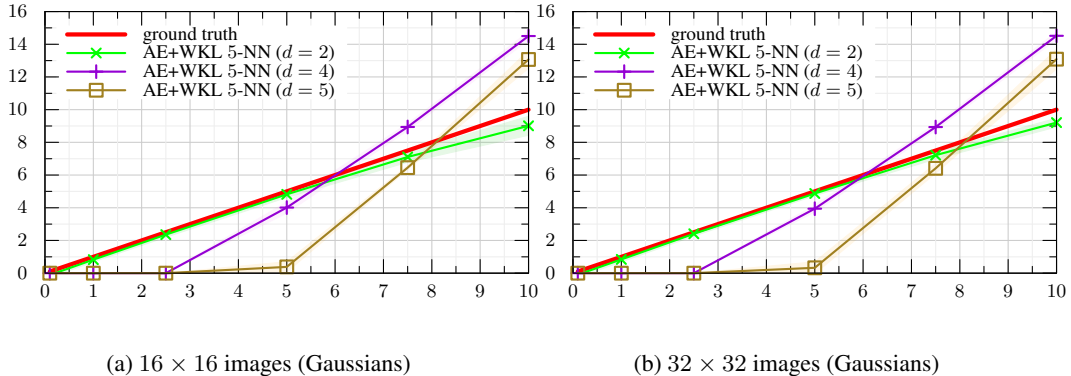


Figure 5: Results for AE+WKL 5-NN for different bottleneck dimensionality. Along  $x$  axes is  $I(X_0; X_1)$ , along  $y$  axes is MI estimate  $\hat{I}(X_0; X_1)$ . We plot 99% asymptotic CIs acquired from different seed runs (5 seeds in total).

Method Type		GT																																																																																																																																																																																																																																																																																																																																																																																																																																																																																																																																																																																																																																																																																																																				
Bridge Matching		InfoBridge																																																																																																																																																																																																																																																																																																																																																																																																																																																																																																																																																																																																																																																																																																																				
Flow	NNVF	0.18	0.40	0.30	0.55	0.41	0.41	0.41	0.96	1.01	1.01	1.02	0.29	0.99	1.27	1.01	0.41	1.02	0.58	1.52	0.40	0.95	0.97	1.02	0.80	0.48	0.58	0.90	0.97	1.01	$\infty$	$\infty$	$\infty$	0.45	0.23	-0.43	0.43	0.16	1.54	0.25	0.41																																																																																																																																																																																																																																																																																																																																																																																																																																																																																																																																																																																																																																																																													
	JVF	0.0	0.0	0.0	0.0	0.41	0.41	0.41	1.02	1.02	1.02	1.02	0.29	1.03	1.29	1.02	0.41	1.02	0.59	1.65	0.41	1.02	1.02	1.02	0.83	0.27	0.41	0.95	0.87	0.90	1.82	2.66	0.01	0.09	0.0	0.11	0.0	0.03	1.55	0.18	0.41																																																																																																																																																																																																																																																																																																																																																																																																																																																																																																																																																																																																																																																																													
	MINDE-j ( $\sigma = 1$ )	0.21	0.40	0.26	0.40	0.41	0.41	0.41	1.10	1.01	1.00	1.01	0.29	0.91	1.18	1.00	0.42	1.00	0.59	1.72	0.40	0.96	0.96	0.99	0.87	0.90	0.90	0.95	0.95	0.98	0.17	0.35	0.18	0.25	0.17	0.47	0.29	0.49	1.65	0.31	0.41																																																																																																																																																																																																																																																																																																																																																																																																																																																																																																																																																																																																																																																																													
	MINDE-j	0.22	0.42	0.28	0.42	0.41	0.42	0.42	1.19	1.02	1.02	1.02	0.29	0.99	1.31	1.02	0.41	1.01	0.59	1.73	0.41	1.07	0.99	0.99	0.95	0.92	0.93	1.07	0.99	0.98	0.13	0.24	0.20	0.30	0.18	0.48	0.31	0.40	1.67	0.31	0.42																																																																																																																																																																																																																																																																																																																																																																																																																																																																																																																																																																																																																																																																													
Diffusion	MINDE-c ( $\sigma = 1$ )	0.21	0.42	0.27	0.42	0.41	0.41	0.41	0.96	1.00	0.99	1.01	0.29	1.00	1.26	1.01	0.41	1.01	0.59	1.62	0.40	0.94	0.97	0.95	0.92	0.94	0.93	0.96	0.94	0.13	0.28	0.18	0.29	0.18	0.42	0.30	0.32	1.67	0.31	0.41																																																																																																																																																																																																																																																																																																																																																																																																																																																																																																																																																																																																																																																																														
	MINDE-c	0.21	0.42	0.28	0.42	0.41	0.41	0.41	1.00	1.01	1.01	1.01	0.29	1.00	1.27	1.01	0.41	1.01	0.59	1.60	0.40	0.98	0.99	0.98	0.92	0.94	0.94	0.98	0.98	0.14	0.26	0.19	0.28	0.17	0.44	0.29	0.40	1.66	0.31	0.41																																																																																																																																																																																																																																																																																																																																																																																																																																																																																																																																																																																																																																																																														
	MINNE	0.23	0.38	0.24	0.36	0.40	0.41	0.41	0.96	0.99	0.98	1.01	0.30	0.99	1.28	1.01	0.41	1.00	0.59	1.60	0.39	0.88	0.90	0.90	0.83	0.70	0.65	0.88	0.89	0.87	0.02	0.01	0.12	0.12	0.13	0.16	0.22	0.39	1.66	0.32	0.41																																																																																																																																																																																																																																																																																																																																																																																																																																																																																																																																																																																																																																																																													
	InfoNCE	0.22	0.41	0.27	0.40	0.41	0.41	0.41	0.98	1.01	1.01	1.02	0.29	0.99	1.28	1.01	0.41	1.02	0.59	1.61	0.40	0.92	0.98	0.99	0.83	0.84	0.82	0.92	0.96	0.96	0.15	0.30	0.18	0.27	0.17	0.41	0.28	0.40	1.69	0.32	0.41																																																																																																																																																																																																																																																																																																																																																																																																																																																																																																																																																																																																																																																																													
Classical	D-V	0.22	0.41	0.27	0.40	0.41	0.41	0.41	0.98	1.01	1.01	1.02	0.29	0.99	1.28	1.01	0.41	1.02	0.59	1.61	0.40	0.93	0.98	0.99	0.82	0.82	0.81	0.92	0.96	0.96	0.01	0.05	0.11	0.13	0.15	0.22	0.21	0.40	1.69	0.32	0.41																																																																																																																																																																																																																																																																																																																																																																																																																																																																																																																																																																																																																																																																													
	NNWJ	0.22	0.37	0.27	0.40	0.41	0.41	0.41	0.98	1.01	1.01	1.02	0.29	0.99	1.28	1.01	0.41	1.02	0.59	1.60	0.40	0.93	0.98	0.98	0.82	0.82	0.80	0.92	0.95	0.96	0.03	0.02	0.04	-0.63	0.12	0.12	0.21	0.40	1.69	0.32	0.42																																																																																																																																																																																																																																																																																																																																																																																																																																																																																																																																																																																																																																																																													
	KSW	0.22	0.38	0.19	0.24	0.42	0.42	0.42	0.42	0.42	0.42	0.17	0.87	0.66	1.03	0.29	0.20	1.07	0.95	0.41	0.74	0.57	1.28	0.42	0.20	0.92	0.72	0.18	0.71	0.55	0.20	0.90	0.69	0.16	0.22	0.09	0.12	0.07	0.20	0.15	0.42	1.68	0.32	0.42																																																																																																																																																																																																																																																																																																																																																																																																																																																																																																																																																																																																																																																																										
	LNN	0.25	0.89	2.71	6.63	0.41	0.42	0.42	2.68	6.43	1.27	0.65	0.39	2.49	7.27	3.10	7.31	2.38	7.24	0.53	1.20	2.12	2.74	5.48	0.34	1.48	0.29	0.42	0.00	0.00	0.04	0.34	0.41	0.38	0.99	0.95	0.96	1.02	0.29	1.06	1.33	1.02	0.41	1.02	0.60	1.75	3.99	1.00	0.97	0.96	0.86	0.23	0.39	0.99	0.84	0.90	0.33	0.93	0.11	0.13	0.01	0.31	0.02	0.02	1.63	0.19	0.38																																																																																																																																																																																																																																																																																																																																																																																																																																																																																																																																																																																																																																																			
	CCA	0.16	0.48	0.27	0.57	0.37	0.37	0.39	0.67	0.97	0.96	0.95	0.35	0.67	7.83	0.95	0.64	0.94	1.27	16.11	0.37	0.70	0.99	0.95	0.48	0.58	0.56	0.57	0.74	0.77	6.74	7.93	1.78	2.54	0.61	4.24	1.17	1.57	0.11	0.18																																																																																																																																																																																																																																																																																																																																																																																																																																																																																																																																																																																																																																																																														
	DoE(Gaussian)	0.13	0.37	0.21	0.43	0.41	0.35	0.36	0.62	0.92	0.92	0.95	0.34	0.69	7.83	0.95	0.63	0.93	1.27	16.15	0.41	0.78	1.08	1.05	0.47	0.60	0.55	0.67	0.79	0.81	-0.32	2.00	0.46	0.82	0.29	1.48	0.59	1.58	0.08	0.35																																																																																																																																																																																																																																																																																																																																																																																																																																																																																																																																																																																																																																																																														
	DoE(Logistic)																																																																																																																																																																																																																																																																																																																																																																																																																																																																																																																																																																																																																																																																																																																					</